MIMO SELECTION AND MODELING EVALUATIONS FOR INDOOR WIRELESS ENVIRONMENTS

A Thesis
Presented to
The Academic Faculty

by

Lu Dong

In Partial Fulfillment
of the Requirements for the Degree
Doctor of Philosophy in the
School of Electrical and Computer Engineering

Georgia Institute of Technology
December 2007

MIMO SELECTION AND MODELING EVALUATIONS FOR INDOOR WIRELESS ENVIRONMENTS

Approved by:

Professor Mary Ann Ingram,
Committee Chair
School of Electrical and Computer Engineering
Georgia Institute of Technology

Professor John Barry
School of Electrical and Computer Engineering
Georgia Institute of Technology

Professor Mary Ann Ingram, Advisor
School of Electrical and Computer Engineering
Georgia Institute of Technology

Professor Yucel Altunbasak
School of Electrical and Computer Engineering
Georgia Institute of Technology

Professor Gregory Durgin
School of Electrical and Computer Engineering
Georgia Institute of Technology

Professor Wing Suet Li
School of Mathematics
Georgia Institute of Technology

Date Approved: November 9, 2007

To myself,

to Su Su,

the most important person in my life,

and to Meixia Zhang and Jiaqin Dong,

the most supportive parents of the world.

ACKNOWLEDGEMENTS

The completion of this work would not have been possible without the enormous personal and professional support I received from Dr. Mary Ann Ingram, who supervised this research, helped me develop my thinking and theoretical sensitivity, and guided me through the whole research design. She also taught me very specific, invaluable skills of the trade of writing research.

I thank all the members of the dissertation committee, whose unique contributions helped me improve the argument. Special thanks go to Dr. Gregory Durgin, Dr. John Barry, and Dr. Yucel Altunbasak for their careful feedback, which clarified a great deal of confusion and kept me on the right track; their devotion to my research questions and methods and especially for helping me avoid some typical blunders graduate students easily make and for their great comments and encouragement.

Numerous others have helped me through this process. Most notably, I am grateful to all my graduate student colleagues, too many to list. I'd also like to thank all administrative officers for their patience and help. My family accompanied me through this whole process and share all my happiness and sufferings. Thanks go to them. All shortcomings retained in this work in spite of the generous help are my responsibility.

TABLE OF CONTENTS

LIST OF TABLES

LIST OF FIGURES

SUMMARY

Array-to-array, or multiple-input multiple-output (MIMO), links are known to provide extremely high spectral efficiencies in rich multipath environments, such as indoor wireless environments. The selection of a subset of receiver array antennas for a MIMO wireless link has been studied by many as a way to reduce cost and complexity in a MIMO system while providing diversity gain. Combined with a switched multi-beam beamformer, it becomes the beam selection system that can gain high signal-to-interference ratio (SIR) improvement in an interference-limited environment.

The objective of this research is to evaluate the performance of low-complexity antenna or beam subset selection methods for small MIMO networks. The types of networks include (1) point-to-point MIMO links with out-of-system interference, (2) multi-user networks with a single, but possibly spatially distributed access point. We evaluate various selection techniques on measured indoor channels, which has not been done before. We propose a new practical selection metric, the peak-to-trough ratio of orthogonal frequency division multiplexing (OFDM) training symbols. We also compare antenna and beam selection on measured indoor channels under more general conditions than has previously been done. Finally, we consider some channel modeling issues associated with beamformers. We investigate the validity of three types of statistical MIMO channel models. A new beamformer is designed based on the ideal of the "Weichselberger model."

CHAPTER I

INTRODUCTION

Multiple-input and multiple-output (MIMO) systems are known to provide extremely high spectral efficiencies in rich multipath environments [16], such as indoor wireless environments. They are now being used for third-generation cellular systems (WCDMA) and the IEEE 802.11n standard. A MIMO system can be classified as either spatial diversity or spatial multiplexing, based on the transceiver's design strategy. It can also be classified as either point-to-point MIMO or multi-user MIMO, based on its network structure. MIMO-related topics occupy a considerable part of current academic communications research.

Regardless of its use for diversity or spatial multiplexing, any MIMO system's main drawback is the increased complexity and, thus, the cost. While additional antenna elements (patch or dipole antennas) are usually inexpensive, and the additional digital signal processing becomes ever cheaper, the RF elements are expensive and do not follow Moore's law. A MIMO system with Nt- transmit and Nr- receive antennas requires Nt- complete and Nr- complete RF chains, including low-noise amplifiers, downconverters, and analog-to-digital converters, at the transmitter and the receiver, respectively. This thesis focuses on the antenna and beam selection technology, which can well combat such a drawback.

Antenna selection offers a good trade-off between complexity and performance of the MIMO system. It keeps the number of RF branches reasonable and offers selection-diversity gain over a non-selection MIMO system. Selection can be made at the transmitter [21, 25, 44], receiver [23], or both [22] to improve system performance.

Array antennas with switched beamformers have been recognized as effective for

combatting multipath fading of the desired signal and for suppressing interference [37, 49]. Compared with fully adaptive antennas, switched-beam antennas do not have high computation and implementation complexity, but they still can gain high SIR improvement in an interference-limited environment [32]. Also, beamforming digitally with selection has three main advantages: (1) At the transmitter, it reduces the dynamic range requirements on the transmitter; (2) Compared with RF hardware beamforming, it does not have insertion loss [7]; (3) In correlated environments, it gives a performance benefit [36]. The first advantage can be explained as follows. Antenna selection puts all the power through a few selected antenna elements. Beam selection, on the other hand, needs only phase difference between all the antenna elements. So, for beam selection, all the antenna elements have similar transmitted power, which increases the power amplifier's efficiency.

1.1 Research Questions

In this thesis, the performance of low-complexity antenna or beam subset selection for small MIMO networks is evaluated. The types of networks considered include (1) point-to-point MIMO links with out-of-system interference, (2) multi-user networks with a single, but possibly spatially distributed access point. This thesis includes three main research areas, which answer three main questions.

(1) Is there a practical beam selection algorithm that can give both reasonable selection diversity gain and implementation complexity?

(2) How different is the performance between beam selection and antenna selection for different channel scenarios?

(3) Is there a beamformer design that can increase the beam selection performance?

Answering the first question will provide an optional implementation for the beam selection technology in the near future. Answering the second question will help us understand in what kind of situation beam selection technology is valuable, and, what

is the best performance we can get with beam selection. In other words, answers to question 2 will guide the future development of beam selection technology. One such development is to design a novel beamformer, which answers question 3. The idea of such a design process comes after some analysis and research of three MIMO channel models.

The remaining sections of this chapter provide an overview of the three research areas, which include the motivations of the research topics, previous related works and our contributions.

1.2 Peak-to-trough (PTR) Beam Selection Algorithm

This section is related to question 1: Is there a practical beam selection algorithm that can give both reasonable selection diversity gain and implementation complexity?

For the first type of network (point-to-point MIMO links with out-of-system interference), a new selection metric is proposed and the feasibility is proved through experiment. The metric helps to avoid beam-falsing, which is the most serious loss in switched-beam antennas; this occurs when the selected beams are not the best beams. One common method for beam selection is choosing beams with the largest received powers based on the received signal strength indication (RSSI). But, it is possible that the wrong beams will be chosen since RSSI does not distinguish between desired signal and interference. In [32], a dual-metric beam selection algorithm is proposed. The first metric, RSSI, is intended to be measured by an analog detector, while the second metric, bit error rate (BER), could be measured, in theory, in the digital signal processor (DSP). However, BER is not a practical metric. So, a practical "second" metric, which is called the peak-to-trough (PTR) metric, is proposed.

The PTR metric is related to the metric of [34], which is a beam selection method based on signal validation. The idea described in [34] relies on a sequence of unique words periodically embedded in the transmitted symbol sequence. Beams with the

highest cross-correlation with the unique words are selected. For scenarios with uncorrelated interference, the peak-to-trough (PTR) metric is evaluated on the Georgia Electronic Design Center (GEDC) high-speed link prototype. The PTR metric has two main advantages: (1) no channel state information (CSI) is needed, and (2) the metric is robust to frequency-, time-, and sampling-offset. However, this metric cannot be used when interference is caused by users in the same system (the same training structure).

In this thesis, a multi-beam receive system and the principle of the PTR metric beam-selection algorithm are described. Combined with RSSI selection, the PTR metric will select beams that have both good desired signal gain and little probability of including large noise and interference. Analysis and simulation results show that the PTR metric is robust to synchronization offsets for 802.11a and 802.16a waveforms. The dual metric (RSSI and PTR) selection method is a good choice for a MIMO system with high signal-to-noise ratio (SNR) or low signal-to-interference ratio (SIR).

1.3 Comparison of Beam and Antenna Selection

This section is related to question 2: How different is the performance between beam selection and antenna selection for different channel scenarios?

For the second type of network (multi-user networks with a single, but possibly spatially distributed access point), various selection techniques are evaluated, for the first time, over measured indoor channels. Antenna and beam selection are also compared over measured indoor channels. Comparison in this thesis includes three main aspects: (1) different selection metrics (maximum channel capacity (MCC), maximum minimum singular value of the channel matrix (MMSV), or minimum SER (MSER)); (2) different selection types (antenna selection or beam selection); (3) different receive structures (signal (non-distributed) receiver or distributed receivers).

1.3.1 Selection: Metrics, Antennas and Beams

Many selection metrics, such as symbol error rate, channel capacity, eigenvalues of channel matrix, and channel gain (instantaneous SNR), have already been proposed. Although channel gain (instantaneous SNR) is the easiest selection metric for practical implementation, it does not result in good performance improvement. The phase shifts between the antenna elements are the decisive factors and are far more important than instantaneous SNR [35].

The maximum channel capacity (MCC) and the maximum minimum singular value of the channel matrix (MMSV) are two popular practical selection criteria [25]. In [25] and [5], these two criteria are compared in terms of their symbol-error-rate (SER) performance over independent identically distributed (i.i.d.) circular complex Gaussian channels. In [5], these two selection criteria are compared with the minimum SER (MSER) criterion, which also is the optimal selection criterion, over simulated channels. The results described in [5] indicate very little difference between the MCC and MMSV selection criteria in terms of SNR required for a specified SER for the six-select-two receiver selection.

In this thesis, all three criteria (MCC, MMSV, MSER) are compared over measured indoor channels in terms of the symbol error rate (SER).

1.3.2 Comparison of Beam and Antenna Selection

Beam and antenna selection are compared in different measured channels. Although this has been done by others, it was done with an insufficient number of beams or with simulated channels. In [29], beam selection was compared to antenna selection for measured indoor channels, and the beamwidths were consistent with only a four-element array. Based on the MSER criterion, multi-beam beamforming with beam selection was shown via simulation to produce a 16 dB signal-to-interference ratio (SIR) improvement in an interference-limited environment, relative to antenna

selection [32]. In [36], the authors conclude that beam selection can offer a significant advantage for channel capacity in correlated channels.

In this thesis, both correlated and uncorrelated channels are measured. Beam and antenna selection are compared over these measured channels, for both four- and eight-element arrays.

1.3.3 Comparison of Distributed and Non-distributed Receivers

The distributed and non-distributed receivers are also compared in this thesis. In [32], diversity combining with beams suffered because, while both beams exhibited frequency selective fading, either one beam had a much higher average power than the other or the selected beams were adjacent and had correlated fading. This last observation is what provided the motivation for the distributed-beamformer access-point architecture that is considered in this thesis. If the access point can select beams from two significantly separated beamformers, then it should be possible to select two uncorrelated beams with similar average power.

MIMO subchannels formed by beamformers can be expected to vary more in terms of power than MIMO subchannels created only from spatial separation. This is because multipaths typically occur in clusters [26]. Therefore, if a transmit beam and a receive beam both point to the same cluster, the corresponding MIMO subchannel is likely to have a high average power. On the other hand, if one or both beams do not point to a cluster, then there will be very little power associated with that MIMO subchannel. In other words, beams in the latter case are poorly coupled. A similar situation has been observed in MIMO channels formed by dual-polarized antennas [4]. In the line-of-sight (LOS) channels, the coupling is poor between orthogonal polarizations [4]. When K factors are low, poor coupling leads to capacity degradation [4].

The power imbalance problem described above depends on the the degree to which

the beamwidth is matched to the cluster size. Results in [31] show that in low-correlated channels (wide angle spread), narrow beams offer a higher angle diversity gain and less signal fading than the wide beams. Similarly, [41] indicates that angle (i.e., beam) diversity compares closely with traditional space diversity in a complex scattering Rayleigh-fading channel such as an urban mobile radio environment (low-correlated channel). On the other hand, for a Rician-fading channel like a rural environment (high-correlated channel), angle diversity does not work as effectively as space diversity. The main reason for the degraded angle-diversity performance in rural locations is a large mean-signal imbalance on the diversity channels. This difference in mean signal reduces the selection diversity gain on the order of that imbalance.

The distributed access point configuration also brings shadowing effects into the MIMO channel. For MIMO channels with macro-diversity [27], shadowing has been shown to be a more dominating factor than fading correlation [27].

In this thesis, the distributed and non-distributed receivers are compared and the differences are explained based on the knowledge of the above analysis. A new MIMO selection architecture guide, considering both the system complexity and the SER performance, is proposed.

1.4 MIMO Channel Modeling and Beamformer Design

This section is related to question 3: Is there a beamformer design that can increase the beam selection performance?

As a final part of this thesis, some channel modeling issues associated with novel beamformer design are considered. The validity of two types of statistical MIMO channel models, which both have a beamspace-type interpretation, for the measured indoor environment, are investigated. The first is the "virtual channel representation" [43] and the second is a combination of the "virtual channel representation," and the

"Kronecker model" [30], which is called the "Weichselberger model" [47].

In fading MIMO channels, previous studies mostly use i.i.d. Gaussian matrices [15, 16] to represent MIMO channels. The influence of spatial fading correlation on either the TX or the RX side of a wireless MIMO radio link has been addressed in [45], where the one-ring geometric model is proposed. The authors in [45] assume that only spatial fading correlation is responsible for the rank structure of the MIMO channel. In practice, however, the realization of a high MIMO capacity is sensitive not only to the fading correlation, but also to the structure of scattering in the propagation environment. In [9], a "keyhole" model is shown to have zero correlation between the entries of the channel matrix, and yet it has only a single degree of freedom. The authors in [17] show the existence of "pinhole" channels that exhibit low-fading correlation between antennas but still have poor rank properties and hence low capacity. Both "keyhole" and "pinhole" models can be seen as having scattering regions surrounding both the transmit and receive ends, which are separated by a screen with a small hole in the middle.

A simple stochastic MIMO model called the "Kronecker model" has been developed in [30, 40]. This model uses the correlation matrices at the mobile station (MS) and base station (BS) so that results of the previous numerous single-input multiple-output (SIMO) studies can be used as input parameters. But, such a correlation structure is still quite restrictive and can only be justified in scenarios where the scattering is locally rich at either the transmitter or the receiver [47]. Also, [38] shows that realistic indoor MIMO channels cannot be modeled adequately by this approach; channel capacity is underestimated when the number of antennas at one link end becomes larger than two or three. Another drawback of the Kronecker model is that it neglects the statistical interdependence of both link ends.

Eventually, the goal of MIMO channel modeling is to express the underlying spatial structure of the radio environment. An interesting effort, called the "virtual

channel representation," is presented in [43]. The author utilizes a virtual partitioning of the spatial domain to characterize the MIMO channel. A key property of the virtual representation that is exploited is that the components of the virtual channel matrix are approximately independent. With this approximation, the virtual representation allows for a general capacity analysis without the common simplifying assumptions of Gaussian statistics and product-form correlation (Kronecker model) for the channel-matrix elements. But the virtual channel representation restricts the eigenbases of one-sided correlation matrices to predefined DFT matrices. The DFT matrices serve as asymptotically (as the number of antenna elements goes to infinity) optimal eigenfunctions for the channel matrix. However, for a practical number of antenna elements, the approximation of the true eigenbases by the predefined DFT matrices can be rather poor.

Recently, a novel stochastic MIMO channel model was proposed [47]. It combines the advantages of both the Kronecker model and virtual channel representation. It not only considers the correlation at both link ends, but also models their mutual dependence; meanwhile, it adopts the spatial eigenbases to the channel as well as to the array configuration. Furthermore, its mathematical description is simple and concise. This model is called the "Weichselberger model" in this thesis.

The Kronecker model, the virtual channel representation and the Weichselberger model are validated with our measured channel data. A new beamformer is designed based on the ideal of the Weichselberger model. The beam selection performance with the new beamformer is compared to the Butler matrix and optimal beamformer.

1.5 Organization

This thesis is organized as follows: Chapter 1 presents previous related research and the motivations for this thesis. Chapter 2 presents background material and concepts related to this research. Chapter 3 presents the new practical selection metric (PTR

metric) and its performance. Chapter 4 compares beam and antenna selection over measured small MIMO networks and proposes a new MIMO selection architecture for indoor channels. Chapter 5 investigates different MIMO channel models and proposes a novel beamformer design through such investigation. Chapter 6 provides conclusions.

CHAPTER II

BACKGROUND

This chapter provides background information on MIMO systems, their capacity, channel effects, MIMO combine with OFDM, beamforming, selection metrics, and channel modeling.

2.1 MIMO System Introduction

A multiple-input multiple-output (MIMO) system can be classified as either spatial diversity or spatial multiplexing, based on the design strategy of the transceiver. A MIMO system can also be classified as either a point-to-point MIMO or a multi-user MIMO, based on its network structure.

2.1.1 Spatial Diversity

Spatial diversity includes transmit and receive diversity. Because of the well-known research history of receive diversity, only transmit diversity is introduced.

Transmit diversity is a space-time coding technique in which data is spread redundantly across the transmit antenna elements to improve the reliability of a link in the presence of multipath fading. Transmit diversity is particularly useful when the transmitter does not know the channel state information (CSI) and the channel is not reliable. Alamouti proposed a simple space-time block code for transmission with two antennas [3].

The advantages of transmit diversity are that no CSI is required at the transmitter, and the receiver does not need multiple antenna elements to benefit from the diversity gain. The one disadvantage of transmit diversity is that an interference source using transmit diversity creates a number of interference data streams equal to the number

of transmit antenna elements. This type of interference is difficult to suppress.

2.1.2 Spatial Multiplexing

In MIMO links, multiple data streams can be transmitted in parallel. A simple example of spatial multiplexing is a multiple-access cellular network with multiple element arrays (MEAs) at the base stations and a single antenna at each of the mobile units. Another example that has recently generated a great deal of interest and will be studied in this thesis is multiple links with MEAs at both the transmitter and the receiver.

In open-loop (OL) spatial multiplexing, CSI is not exploited at the transmitter, and each antenna element transmits a different data stream with equal power. This is illustrated in Figure 1(a). In closed-loop (CL) spatial multiplexing, as depicted in Figure 1(b), both the transmitter and the receiver adapt to the CSI. Each stream has corresponding transmit and receive antenna patterns.

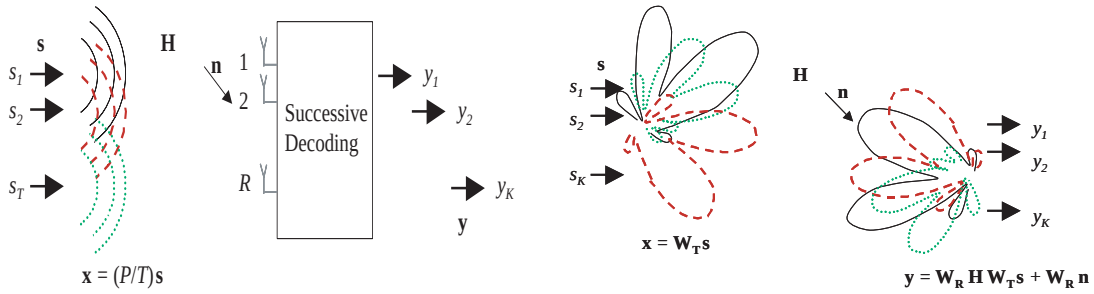

(a) Open-loop spatial multiplexing (b) Closed-loop spatial multiplexing

Figure 1: Spatial multiplexing.

Spatially multiplexed MIMO links have received a great deal of attention because of the tremendous spectral efficiencies that can be achieved with their parallel nature. The channel capacity increases linearly with the number of transmit and receive antennas in rich multipath environments [16], such as indoor wireless channels.

Most practical MIMO systems use the uninformed transmitter or OL approach

[10, 15, 20]. The motivation is that the transmitter does not know CSI, which means a feedback channel is unnecessary. Therefore, the modulation and signal processing at the transmitter have less complexity than in the closed-loop implementation. The original Bell Laboratories Layered Space-Time (BLAST) architecture proposed in [15] is one such approach. It is referred to as diagonal or D-BLAST, since it employs a diagonally-layered coding structure. The code blocks are dispersed across diagonals in space-time. In the simplified vertical scheme (V-BLAST) [20], every antenna radiates an independently encoded equal-rate data stream. The V-BLAST receiver extracts the streams using ordered successive interference cancellation in coordination with a zero-forcing (ZF) or minimum mean-square error (MMSE) filter. Both closed- and open-loop schemes require perfect knowledge of the channel at the receiver.

If no CSI is available at the transmitter, each transmitter antenna must use equal power and rate. The achievable data rate for each transmitted stream is limited by the stream with the least favorable channel. Therefore, depending on the variation in the channel coefficients that each transmit antenna sees, the channel may not support theoretically high data rates with OL-MIMO approaches. The author in [10] states that V-BLAST can attain 50% of the open-loop capacity. More recent research on BLAST schemes presented in [8] and [10] proposes to use limited feedback to adjust the rate of each transmitted data stream. While keeping the transmitted streams independent, a method of power adaptation to better utilize the channel is also proposed in [10] .

2.1.3 Point-to-Point MIMO

A typical point-to-point MIMO is shown in Figure 2(a). In this case, all the N_T transmitter elements carry user data streams to the receiver. Normally, the number of receiver elements N_R should be greater than N_T.

Figure 2(b) shows an example of two point-to-point MIMO links that interfere

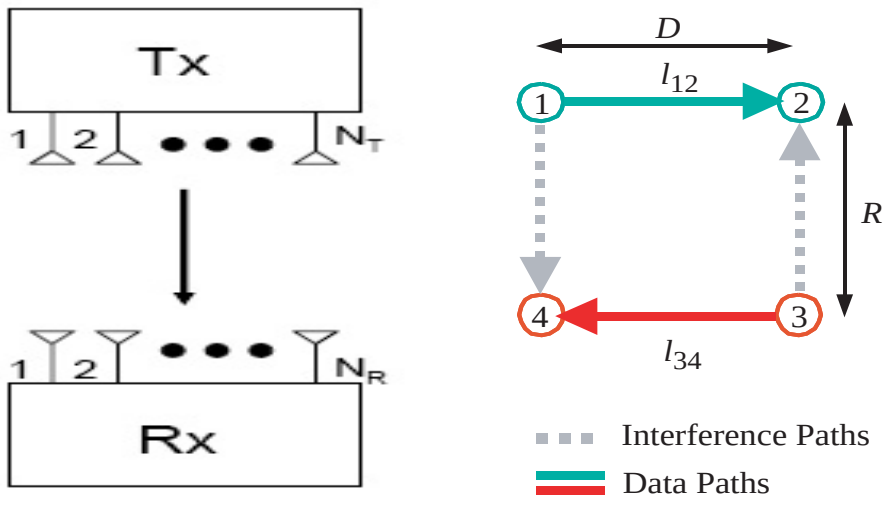

(a) Point-to-point

(b) Two-link ad hoc networks

Figure 2: Point-to-point MIMO.

with each other. The data links are shown by the solid arrows; the interference links are shown by the dashed arrows. Each transmit and receive node has an array antenna with N_T and N_R elements, respectively. The link between nodes i and j is denoted by l_{ij}. The channel gain depends on the distance between the nodes; therefore, as R/D increases, the SIR decreases. This situation occurs in ad hoc networks in which each transceiver node has multiple antennas. Ad hoc networks are multi-hop wireless networks with no fixed infrastructure and no centralized administration. The mobile stations in such networks function as forwarders and participate in the routing process. The nodes communicate by creating a network "on the fly," and the topology can change as the nodes move.

2.1.4 Multi-User MIMO

Sometimes, multiple users need to communicate with a single receiver simultaneously, such as the uplink channels of a wireless local area network (WLAN). When each user with multiple antennas transmits data streams simultaneously, each stream needs to

be detected at the receiver (access point). Normally, the multiple antenna elements at the receiver (access point) are placed in a single position, which is shown in Figure 3(a). But, sometimes, depending on the characteristics of the channel, separating the multiple antenna elements of the receiver in two different positions can offer both macroscopic and microscopic diversity benefits. Figure 3(b) gives an example where the multiple elements of the receiver are distributed in two different positions.

The differences between these two structures is studied in this thesis.

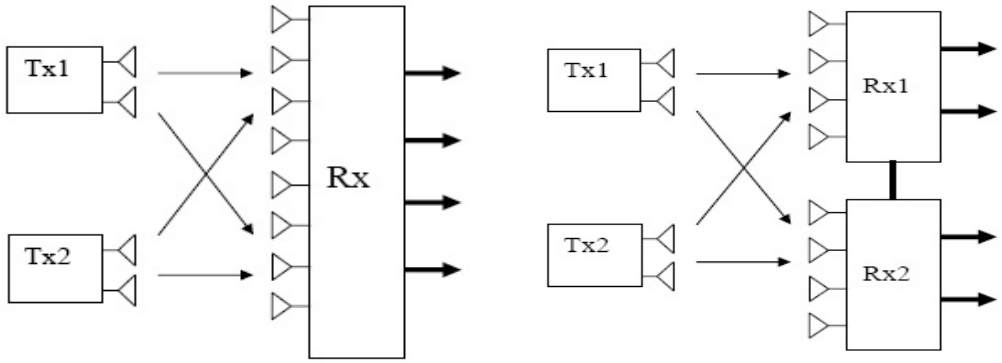

(a) single receiver (b) distributed receiver

Figure 3: Multiuser MIMO.

2.2 MIMO-OFDM System

Orthogonal frequency division multiplexing (OFDM) has become popular for wireless communications. The basic principle of OFDM is to split a high-rate data stream into a number of lower-rate streams that are transmitted simultaneously over a number of subcarriers. Because the symbol duration increases for the lower-rate parallel subcarriers, the relative amount of dispersion in time caused by multipath delay spread is decreased [11, 48].

The OFDM system can be efficiently implemented in discrete time using an inverse fast Fourier transform (IFFT) to act as a modulator and a fast Fourier transform

(FFT) to act as a demodulator. N samples at the output of the OFDM modulator represent an OFDM block. Then, a cyclic prefix consisting of the last G samples of the OFDM block is inserted in front of the OFDM block to form an OFDM symbol. Inter-symbol interference is eliminated almost completely by introducing the guard time between every OFDM symbol. During the guard time, the OFDM waveform is cyclically extended to avoid inter-carrier interference.

At the receiver, the initial G samples from each of the receive blocks are removed and the received downconverted waveforms are demodulated using a FFT.

One example of the 4×4 MIMO-OFDM wireless system is shown in Figure 4.

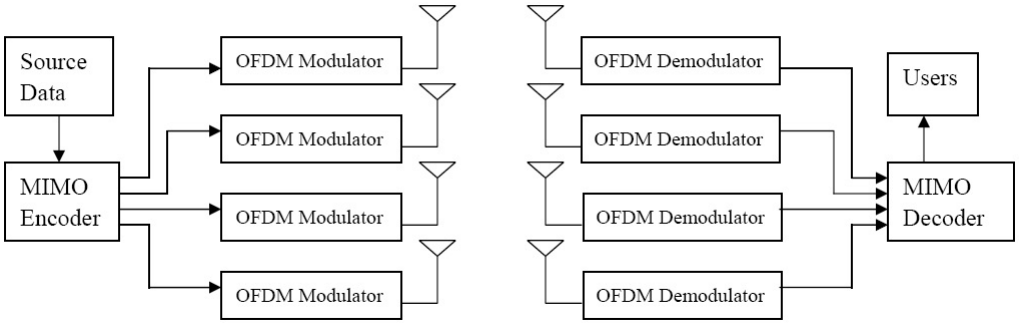

Figure 4: Simulated 4×4 MIMO-OFDM wireless system.

2.3 Capacity of Space Time (ST) Channels

The fundamental limit on the spectral efficiency that can be supported reliably in ST wireless channels is studied in this section. Channel capacity is the maximum error-free data rate that a channel can support. In contrast to scalar AWGN channels, ST channels exhibit fading and encompass a spatial dimension.

2.3.1 Capacity of the Frequency Flat Deterministic MIMO Channel

A MIMO channel is assumed to have N_T transmit antennas and N_R receive antennas and is flat-fading over a 1 Hz bandwidth. Denoting the $N_R \times N_T$ channel transfer

matrix by $\mathbf{H}$, the input-output relation for such MIMO channel is given by

$$\mathbf{y} = \sqrt{\frac{E_s}{N_T}}\mathbf{H}\mathbf{s} + \mathbf{n}, \tag{1}$$

where $\mathbf{y}$ is the $N_R \times 1$ received signal vector, $\mathbf{s}$ is the $N_T \times 1$ transmitted signal vector, $\mathbf{n}$ is the zero-mean circularly symmetric complex Gaussian (ZMCSCG) noise with covariance matrix $\mathbf{E}\{\mathbf{n}\mathbf{n}^H\} = n_0\mathbf{I}_{N_R}$, and E_s is the total average energy available at the transmitter over a symbol period (this equals the total average transmit power since the symbol period is one second). The covariance matrix of $\mathbf{s}$, $\mathbf{R}_{ss} = \mathbf{E}\{\mathbf{s}\mathbf{s}^H\}$, ($\mathbf{s}$ is assumed to have zero mean) must satisfy $Tr(\mathbf{R}_{ss}) = N_T$ to constrain the total average energy transmitted over a symbol period.

The capacity of the MIMO channel is given by

$$\mathbf{C} = \max_{Tr(\mathbf{R}_{ss})=N_T} \log_2 \det(\mathbf{I}_{N_R} + \frac{E_s}{N_T n_0}\mathbf{H}\mathbf{R}_{ss}\mathbf{H}^H)\ bps/Hz. \tag{2}$$

2.3.2 Channel Unknown to the Transmitter

If the channel has no preferred direction and is completely unknown to the transmitter, the signals are independent and equi-powered at the transmit antennas, i.e., $\mathbf{R}_{ss} = \mathbf{I}_{N_T}$. The capacity of the MIMO channel in the absence of CSI at the transmitter is given by

$$\mathbf{C} = \log_2 \det(\mathbf{I}_{N_R} + \frac{E_s}{N_T n_0}\mathbf{H}\mathbf{H}^H). \tag{3}$$

Since a genie with channel knowledge can choose a signal covariance matrix that outperforms $\mathbf{R}_{ss} = \mathbf{I}_{N_T}$, this equation is not the Shannon capacity in the true sense. Given that $\mathbf{H}\mathbf{H}^H = \mathbf{Q}\mathbf{\Lambda}\mathbf{Q}^H$, using the identity $\det(\mathbf{I}_m + \mathbf{A}\mathbf{B}) = \det(\mathbf{I}_n + \mathbf{B}\mathbf{A})$ for matrices $\mathbf{A}$ $(m \times n)$ and $\mathbf{B}$ $(n \times m)$ and $\mathbf{Q}^H\mathbf{Q} = \mathbf{I}_{N_R}$, equation (3) can be simplified to

$$\mathbf{C} = \log_2 \det(\mathbf{I}_{N_R} + \frac{E_s}{N_T n_0}\mathbf{\Lambda}) = \sum_{i=1}^{r} \log_2(1 + \frac{E_s}{N_T n_0}\lambda_i), \tag{4}$$

where r is the rank of the channel, and λ_i $(i = 1, 2, ..., r)$ are the positive eigenvalues of $\mathbf{H}\mathbf{H}^H$. This equation expresses the capacity of the MIMO channel as the sum of

the capacities of r SISO channels, each having power gain λ_i and transmit power E_s/N_T.

2.3.3 Channel Known to the Transmitter

CSI at the transmitter can be maintained via feedback from the receiver or through the reciprocity principle in a duplex system. When the channel is known at both the transmitter and the receiver, the individual channel modes may be accessed through linear processing at the transmitter and the receiver [15].

Considering the singular value decomposition of channel matrix $\mathbf{H} = \mathbf{U}\mathbf{\Sigma}\mathbf{V}^H$, equation (1) changes to

$$\mathbf{y} = \sqrt{\frac{E_s}{N_T}}\mathbf{U}\mathbf{\Sigma}\mathbf{V}^H\mathbf{s} + \mathbf{n}, \tag{5}$$

With $\widetilde{\mathbf{y}} = \mathbf{U}^H\mathbf{y}$, $\widetilde{\mathbf{s}} = \mathbf{V}^H\mathbf{s}$, and $\widetilde{\mathbf{n}} = \mathbf{U}^H\mathbf{n}$, the effective input-output relation for this system is given by

$$\widetilde{\mathbf{y}} = \sqrt{\frac{E_s}{N_T}}\mathbf{\Sigma}\widetilde{\mathbf{s}} + \widetilde{\mathbf{n}}, \tag{6}$$

where $\widetilde{\mathbf{y}}$ is the transformed received signal vector with dimension $r \times 1$ and $\widetilde{\mathbf{n}}$ is the ZMCSCG $r \times 1$ transformed noise vector with covariance matrix $\mathbf{E}\{\widetilde{\mathbf{n}}\widetilde{\mathbf{n}}^H\} = n_0\mathbf{I}_{N_R}$. The rank of the channel $\mathbf{H}$ is r. The vector $\widetilde{\mathbf{s}}$ must satisfy $\mathbf{E}\{\widetilde{\mathbf{s}}\widetilde{\mathbf{s}}^H\} = N_T$. Equation (6) shows that with CSI at the transmitter, $\mathbf{H}$ can be explicitly decomposed into r parallel SISO channels satisfying

$$\widetilde{\mathrm{y}}_i = \sqrt{\frac{E_s}{N_T}}\sqrt{\lambda_i}\widetilde{\mathrm{s}}_i + \widetilde{\mathrm{n}}_i, \;\; i = 1, 2, ..., r. \tag{7}$$

The capacity of the MIMO channel is the sum of the individual parallel SISO channel capacities and is given by

$$\mathbf{C} = \sum_{i=1}^{r} \log_2(1 + \frac{E_s\gamma_i}{N_T n_0}\lambda_i), \tag{8}$$

where $\gamma_i = \mathbf{E}\{|\mathrm{s}_i|^2\}$ $(i = 1, 2, ..., r)$ reflects the transmit energy in the ith subchannel and satisfies $\sum_{i=1}^{r}\gamma_i = N_T$.

Since the transmitter can allocate variable energy across the subchannels, the mutual information maximization problem now becomes

$$\mathbf{C} = \max_{\sum_{i=1}^{r} \gamma_i = N_T} \sum_{i=1}^{r} \log_2(1 + \frac{E_s \gamma_i}{N_T n_0} \lambda_i). \tag{9}$$

The objective function for the maximization is concave with the variables γ_i ($i = 1, 2, ..., r$) and can be maximized using the Lagrangian method. The optimal energy allocation policy, γ_i^{opt}, satisfies

$$\gamma_i^{opt} = (\mu - \frac{N_T n_0}{E_s \lambda_i})_+, \ i = 1, 2, ..., r, \tag{10}$$

where μ is a constant to let $\sum_{i=1}^{r} \gamma_i^{opt} = N_T$ and $(x)_+$ implies

$$(x)_+ = \begin{cases} x & \text{if} \quad x \geq 0 \\ 0 & \text{if} \quad x < 0. \end{cases} \tag{11}$$

2.3.4 Influence of Fading Correlation, Rician Fading on MIMO Capacity

A MIMO channel is represented by $\mathbf{H}_w$ if the environment is rich scattering and the antenna spacing is sufficiently large at the transmitter and the receiver. In practice, however, the $\mathbf{H}_w$ assumption may not be true for several reasons: insufficient scattering or spacing between antennas causing the fading to be correlated; the use of polarized antennas, which leads to gain imbalances between the elements of $\mathbf{H}$; or the presence of a LOS component that causes Rician fading. It needs to be noted that the channel matrices $\mathbf{H}$ and $\mathbf{H}_w$ here represent random MIMO channels instead of sample deterministic channels in the previous sections.

The effects of spatial fading correlation for a Rayleigh flat-fading channel can be reasonably captured by modeling the MIMO channels $\mathbf{H}$ as

$$\mathbf{H} = \mathbf{R}_r^{1/2} \mathbf{H}_w \mathbf{R}_t^{1/2}, \tag{12}$$

where the matrices $\mathbf{R}_r$ and $\mathbf{R}_t$ are positive definite Hermitian matrices that specify the receive and the transmit correlations, respectively. Furthermore, $\mathbf{R}_r$ and $\mathbf{R}_t$

are normalized so that $\mathbf{E}\{|h_{i,j}|^2\} = 1$. The capacity of the MIMO channel in the presence of spatial fading correlation without CSI at the transmitter follows from simple substitution:

$$\mathbf{C} = \log_2 \det(\mathbf{I}_{N_R} + \frac{\rho}{N_T}\mathbf{R}_r^{1/2}\mathbf{H}_w\mathbf{R}_t\mathbf{H}_w^H\mathbf{R}_t^{H/2}), \tag{13}$$

where ρ is the average SNR at the receiver. Assume that $N_R = N_T = N$ and the receive and the transmit correlation matrices $\mathbf{R}_r$ and $\mathbf{R}_t$ are full rank. For high SNR, the capacity of the MIMO channel can be written as

$$\mathbf{C} \approx \log_2 \det(\frac{\rho}{N_T}\mathbf{H}_w\mathbf{H}_w^H) + \log_2 \det(\mathbf{R}_r) + \log_2 \det(\mathbf{R}_t). \tag{14}$$

It is clear that $\mathbf{R}_r$ and $\mathbf{R}_t$ have the same impact on the capacity of the MIMO channel. The eigenvalues of $\mathbf{R}_r$, $\lambda_i(\mathbf{R}_r)$ $(i = 1, 2, ..., N)$ are constrained such that $\sum_{i=1}^{N} \lambda_i(\mathbf{R}_r) = N$. The arithmetic mean-geometric inequality implies

$$\prod_{i=1}^{N} \lambda_i(\mathbf{R}_r) \leq 1. \tag{15}$$

With $\det(\mathbf{R}_r) = \prod_{i=1}^{N} \lambda_i(\mathbf{R}_r)$, it comes out $\log_2 \det(\mathbf{R}_r) \leq 0$, and the equality happens only if all eigenvalues of $\mathbf{R}_r$ are equal, i.e., $\mathbf{R}_r = \mathbf{I}_N$. Hence, fading signal correlation is detrimental to MIMO capacity. The loss in ergodic or outrage capacity at high SNR is given by $(\log_2 \det(\mathbf{R}_r) + \log_2 \det(\mathbf{R}_t))$ bps/Hz.

The MIMO channel in the presence of Rician fading can be modeled as the sum of a fixed (LOS) matrix and a fading matrix as follows:

$$\mathbf{H} = \sqrt{\frac{K}{1+K}}\overline{\mathbf{H}} + \sqrt{\frac{1}{1+K}}\mathbf{H}_w, \tag{16}$$

where $\sqrt{K/(1+K)}\overline{\mathbf{H}}$ is the fixed component of the channel and $\sqrt{1/(1+K)}\mathbf{H}_w$ is the fading component of the channel. Symbol K represents the Rician factor of the channel, which is the ratio of the total power in the fixed component to the power in the fading component. The geometry of the fixed component of the channel matrix $\overline{\mathbf{H}}$ plays a critical role for channel capacity calculation at a high K factor. Normally,

the more likely $\overline{\mathbf{H}}$ is to an orthogonal matrix, the higher capacity we can get. Further details can be found in [18, 19].

2.4 Butler Matrix, Antenna, and Beam Selection

A MIMO link with multiple antennas can be changed to a MIMO link with multiple beams by simply inserting a multi-beam beamformer (MBBF), such as a Butler matrix, between the antennas and the switch. To avoid high complexity and still get good diversity gain, a few antennas or beams can be selected from the total number of multiple antennas or beams.

Figure 5 gives an example for antenna or beam selection in a 4×4 MIMO system.

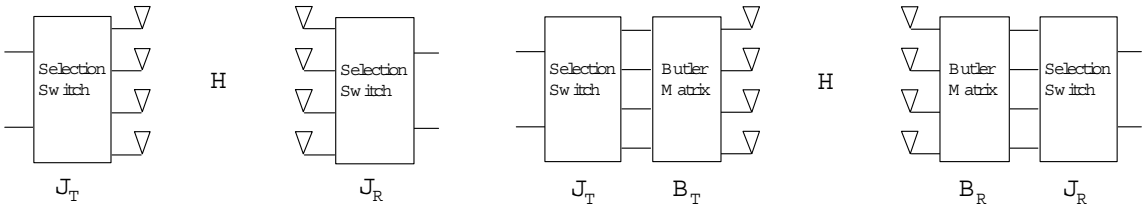

(a) Antenna selection MIMO System

(b) Beam selection MIMO System

Figure 5: MIMO selection system with and without MBBF.

Assuming the numbers of transmit and receive antennas are N_T and N_R, respectively, the measured channel matrix, denoted as H, is an $N_R \times N_T$ matrix, which is noise-normalized before being further employed by the beam and antenna selection method. Assuming the numbers of selected transmit and receive antennas are n_T and n_R, respectively, the MIMO channel matrices after antenna selection and beam selection are given by

$$H_{ant} = J_R H J_T^H, \tag{17}$$

and

$$H_{beam} = J_R B_R H B_T^H J_T^H, \tag{18}$$

respectively, where x^H means transpose conjugate of x. The component matrices are indicated in Figure 5 and explained as follows. Matrices $J_R \in R_{n_R \times N_R}$ and $J_T \in R_{n_T \times N_T}$ are the lossless selection matrices at both ends; matrices $B_R = [B_R^1, B_R^2, \cdots B_R^{N_R}]$ and $B_T^H = [B_T^1, B_T^2, \cdots B_T^{N_T}]$ are the lossless receive and transmit Butler matrices [39]. The m^{th} columns of B_R and B_T^H are

$$B_R^m(n) = \frac{1}{\sqrt{N_R}} e^{\frac{j\pi(m-1)[-(N_R-1)+2(n-1)]}{N_R}}, n = 1 \cdots N_R, \tag{19}$$

and

$$B_T^m(n) = \frac{1}{\sqrt{N_T}} e^{\frac{-j\pi(n-1)[-(N_T-1)+2(m-1)]}{N_T}}, n = 1 \cdots N_T. \tag{20}$$

respectively.

2.5 Selection Metrics Introduction

The optimal selection metric is obviously the minimum symbol error rate (MSER). But, it is not a practical metric because of the time-consuming calculation. Normally, the channel capacity and the singular value of a channel matrix are used for practical selection metrics [5, 25].

2.5.1 Maximum Channel Capacity (MCC) Metric

In an open-loop MIMO system, the power is evenly allocated to each transmit antenna. With this assumption, it is well known that the capacity of the channel without interference is calculated as

$$\mathbf{C} = \log_2 \det(I + \frac{\rho}{n_T} H H^H). \tag{21}$$

For the channels with multiple point-to-point MIMO links that interfere each other, suppose the correlation matrix of the interference is R_{int}; the capacity is calculated as follows [6]:

$$\mathbf{C_{int}} = \log_2 \det(I + \frac{\rho}{n_T} \widetilde{H} \widetilde{H}^H), \tag{22}$$

where $\widetilde{H} = (I + R_{int})^{-1/2} H$. The beams or antennas are selected to maximize the channel capacity (MCC).

2.5.2 Maximum Minimum Singular Value (MMSV) Metric

Consider a spatial multiplexing system with N_T transmit antennas, N_R receive antennas, and a $1 : M(N_T > M, N_R \geq M)$ multiplexer. Within one symbol time, M input symbols are multiplexed to produce the $(M \times 1)$ vector symbol $\mathbf{s}_n$ for transmission over M transmit antennas. A subset of $M \leq N_T$ transmit antennas is determined by a selection algorithm operating at the receiver, which indicates to the transmitter the optimal subset $p \in P$, where P is the set of all possible $\begin{pmatrix} N_T \\ M \end{pmatrix}$ subsets of transmit antennas.

$\mathbf{H}$ denotes the $N_R \times N_T$ channel matrix and $\mathbf{H}_p$ denotes the $N_R \times M$ submatrix corresponding to the transmit antenna subset p. The corresponding received signal, at discrete-time n, after matched filter and sampling is

$$\mathbf{y}_n = \sqrt{\frac{E_s}{M}}\mathbf{H}_p\mathbf{s}_n + \mathbf{n}, \tag{23}$$

where $\mathbf{y}_n$ and the noise $\mathbf{n}$ are $N_R \times 1$ vectors. The maximum total power transmitted on M antennas at one symbol time is E_s assuming that $\mathbf{s}_n$ is normalized such that $tr(\mathbf{E}\{\mathbf{s}_n\mathbf{s}_n^H\}) = M$. The symbols on all substreams are derived from the same constellation.

R denotes the desired spectral efficiency, $M_{sm} = 2^{R/M}$ is the number of points in the per-antenna constellation, $\mathbf{y}$ is the received data vector at sample time n, $\mathbf{s}$ is the transmitted vector symbol, and S_{SM} is the set of all possible transmitted vectors $\mathbf{s}$. The size of S_{SM} is $M_{SM} = |S_{SM}| = M_{sm}^M$. In the analysis, the channel $\mathbf{H}_p$, which consists of the appropriate columns of $\mathbf{H}$, is considered to be dictated by the subset indicated by p.

From the above definitions, the maximum likelihood (ML) estimate of the transmitted vector $\mathbf{s}$ is

$$\widehat{\mathbf{s}} = arg \min_{\mathbf{s} \in S_{SM}} \parallel x - \sqrt{\frac{E_s}{M}}\mathbf{H}_p\mathbf{s} \parallel^2 . \tag{24}$$

This computation requires a search over all the M_{SM} possible transmitted vectors.

At a high SNR, BER is upper bounded by using the union bound, which is a function of $d^2_{min,SM}$. $d^2_{min,SM}$ is the squared minimum distance of the receive constellation, which is defined as $\{\mathbf{H}_p\mathbf{s}|\mathbf{s} \in S_{SM}\}$ [24].

Suppose that $\mathbf{s}_i \in S_{SM}$, $\mathbf{s}_j \in S_{SM}$, $\mathbf{s}_i \neq \mathbf{s}_j$. The squared minimum distance of the receive constellation is defined as

$$d^2_{min,SM} = \min_{\mathbf{s}_i,\mathbf{s}_j \in S_{SM}, \mathbf{s}_i \neq \mathbf{s}_j} \frac{\parallel H_p(\mathbf{s}_i - \mathbf{s}_j) \parallel^2}{M}. \tag{25}$$

Because of the linear transformation by the channel, the distance properties of $\mathbf{s}_i$ are not preserved unless $\mathbf{H}_p$ is unitary.

The computation in (25) requires a search over $S_{SM}(S_{SM} - 1)$ vectors, which can be prohibitive for larger constellations. Therefore, it is useful to develop a lower bound on $d^2_{min,SM}$, which is presented in [24].

$\mathbf{e}_{min}$ is the right singular vector of $\mathbf{H}_p$ corresponding to the smallest singular value λ_{min}. Assume $\mathbf{e}_{ij} = \mathbf{s}_i - \mathbf{s}_j$ and the minimum squared distance of the transmit constellation is $d^2_{min,sm} = \min_{\mathbf{s}_i,\mathbf{s}_j \in S_{SM}} \parallel \mathbf{s}_i - \mathbf{s}_j \parallel^2$. Then, the following relationship can be deduced:

$$\min_{\mathbf{s}_i,\mathbf{s}_j \in S_{SM}} \parallel \mathbf{H}_p\mathbf{e}_{ij} \parallel^2 = \min_{\mathbf{s}_i,\mathbf{s}_j \in S_{SM}} \frac{\parallel \mathbf{H}_p\mathbf{e}_{ij} \parallel_2^2}{\parallel \mathbf{e}_{ij} \parallel^2} \parallel \mathbf{e}_{ij} \parallel^2 \geq \lambda^2_{min}(p) d^2_{min,sm}. \tag{26}$$

The inequality in the relationship follows from Rayleigh-Ritz theorem, i.e., $\frac{\|\mathbf{H}_p\mathbf{e}_{ij}\|_2^2}{\|\mathbf{e}_{ij}\|^2} \geq \min_{\mathbf{x}} \frac{\|\mathbf{H}_p\mathbf{x}\|_2^2}{\|\mathbf{x}\|^2} = \lambda^2_{min}(p)$ and $d_{min,sm} = \min_{\mathbf{x}} \parallel \mathbf{e}_{ij} \parallel$. The equality occurs if there exists an $\mathbf{s}_i - \mathbf{s}_j$, which is a scalar multiple of the minimum right singular vector $\mathbf{H}_p$. Using (25) and (26), the desired result is obtained as

$$d^2_{min,SM} \geq \frac{\lambda^2_L(p) d^2_{min,sm}}{M}. \tag{27}$$

Using (27), the probability of symbol error can be upper bounded using the union bound as

$$P_{SM} < (|S_{SM}| - 1) Q\left(\sqrt{\frac{E_s}{2N_0} \frac{\lambda^2_L d^2_{min,sm}}{M}}\right). \tag{28}$$

Therefore, from (28), the maximum minimum singular value (MMSV) is a useful metric.

2.6 MIMO Channel Modeling

In this section, three MIMO channel models are introduced. The first one is the Kronecker model. This model does not describe the joint spatial structure of the channel. In other words, it does not have beamspace-type interpretation for the measured channel. The second one is the virtual channel representation. The third one is the Weichselberger model, which utilizes the knowledge of the Kronecker model and virtual channel representation.

The spatial correlation on one link end is denoted by a one-side correlation matrix. Because the two link ends cannot be considered independent, the one-side correlation matrices have to be parameterized by the statistical signal properties of the other link ends.

$$\mathbf{R_{RX,Q_{TX}}} = \mathbf{E_H}\{\mathbf{HQ_{TX}H^H}\},\ \mathbf{R_{TX,Q_{RX}}} = \mathbf{E_H}\{\mathbf{H^T Q_{RX} H^*}\}, \tag{29}$$

where $\mathbf{Q_{RX}}$ and $\mathbf{Q_{TX}}$ are the spatial signal covariance matrices of the receiver and transmitter, respectively.

If the two link ends are independent of each other as the Kronecker model assumes, the signal covariance of the other link end is spatially white. So, the one-side correlation matrices become $\mathbf{R_{RX}} = \mathbf{E_H}\{\mathbf{HH^H}\}$ and $\mathbf{R_{TX}} = \mathbf{E_H}\{\mathbf{H^T H^*}\}$. Their eigenbases are denoted by $\mathbf{U_{RX}}$ and $\mathbf{U_{TX}}$. The vectors $\overrightarrow{\lambda}_{\mathbf{RX}}$ and $\overrightarrow{\lambda}_{\mathbf{TX}}$ consist of the square roots of the eigenvalues of $\mathbf{R_{RX}}$ and $\mathbf{R_{TX}}$, respectively.

2.6.1 The Kronecker MIMO Channel Model

The basic assumption of the Kronecker model is that the full channel correlation matrix can be modeled by the Kronecker product of the transmit and receive correlation

matrix [30]. This leads to the stochastic channel model:

$$\mathbf{H_{kron}} = \frac{1}{\sqrt{tr\{\mathbf{R_{RX}}\}}}\mathbf{R_{RX}}^{1/2}\mathbf{G}(\mathbf{R_{TX}}^{1/2})^T, \tag{30}$$

where G is a random matrix with independent identically distributed (i.i.d) complex Gaussian entries. Equation (30) can be equivalently expressed as

$$\mathbf{H_{kron}} = \frac{1}{\sqrt{tr\{\mathbf{R_{RX}}\}}}\mathbf{U_{RX}}((\overrightarrow{\lambda}_{\mathbf{RX}}\overrightarrow{\lambda}_{\mathbf{TX}}^{\ T}) \odot \mathbf{G})\mathbf{U_{TX}^T}, \tag{31}$$

where $\odot$ denotes the element-wise product of two matrices.

2.6.2 The Virtual Channel Representation MIMO Channel Model

The virtual channel representation can be written as

$$\mathbf{H_{virt}} = \mathbf{A_{RX}}(\widetilde{\mathbf{\Omega}}_{\mathbf{virt}} \odot \mathbf{G})\mathbf{A_{TX}^T}, \tag{32}$$

where $\mathbf{G}$ is the same i.i.d matrix as before. The matrices $\mathbf{A_{RX}}$ and $\mathbf{A_{TX}}$ are channel-independent discrete Fourier transform (DFT) matrices of size $N_R \times N_R$ and $N_T \times N_T$, respectively. The virtual channel representation restricts the eigenbases of one-sided correlation matrices to predefined DFT matrices (the Butler matrix is one such example). Because the DFT matrix associates a basis vector with a direction, this model does describe the joint spatial structure. For a practical number of antenna elements, the approximation of the true eigenbases by the predefined DFT matrices can be rather poor [43]. The $\widetilde{\mathbf{\Omega}}_{\mathbf{virt}}$ is the element-wise square root of the power coupling matrix $\mathbf{\Omega_{virt}}$. Based on measurements, it can be simply estimated as

$$\mathbf{\Omega_{virt}} = \mathbf{E_H}\{(\mathbf{A_{RX}^H H A_{TX}^*}) \odot (\mathbf{A_{RX}^T H^* A_{TX}})\}. \tag{33}$$

2.6.3 The Weichselberger MIMO Channel Model

The Weichselberger model is a combination of both the Kronecker model and virtual channel representation [47]. It describes the joint spatial structure of the channel as

the virtual channel representation and adopts the spatial eigenbases to the channel as in the Kronecker model. The channel matrices are generated by

$$\mathbf{H_{weich}} = \mathbf{U_{RX}}(\widetilde{\mathbf{\Omega}} \odot \mathbf{G})\mathbf{U_{TX}^{T}}, \tag{34}$$

where $\mathbf{U_{RX}}$, $\mathbf{U_{TX}}$, and $\mathbf{G}$ are the same as before. The $\widetilde{\mathbf{\Omega}}$ is the element-wise square root of the power coupling matrix $\mathbf{\Omega}$, which can be estimated as

$$\mathbf{\Omega} = \mathbf{E_H}\{(\mathbf{U_{RX}^{H}}\mathbf{H}\mathbf{U_{TX}^{*}}) \odot (\mathbf{U_{RX}^{T}}\mathbf{H^{*}}\mathbf{U_{TX}})\}. \tag{35}$$

CHAPTER III

BEAM SELECTION WITH SIGNAL STRENGTH AND PEAK-TO-TROUGH RATIO OF OFDM TRAINING SEQUENCES

3.1 Introduction

From the previous chapters, we already know that switched-beam antennas do not have high computation and implementation complexity, but still can gain high signal-to-interference ratio (SIR) improvement in an interference-limited environment [32]. The multiple selected beams can be used for diversity combining and for multiple-input multiple-output (MIMO) links. However, beam-falsing, which is the most serious loss in switched-beam antennas, occurs because the selected beams may not be the best beams. One common method for beam selection is choosing beams with the largest received powers based on the RSSI. But it is possible that the wrong beams will be chosen since RSSI does not distinguish between desired signal and interference.

In [32], a dual-metric beam selection algorithm is proposed. The first metric, RSSI, is intended to be measured by an analog detector, while the second metric, bit error rate (BER), could be measured, in theory, in the digital signal processor (DSP). The goal in [32], as it is here, is to make a selection using only two full radio chains. However, BER is not a practical metric because it requires a time-consuming calculation. It is the goal of this chapter to present a practical "second" metric, which we call the peak-to-trough (PTR) metric.

The PTR metric is related to the metric of [34], which is a beam selection method based on signal validation. The idea described in [34] relies on a sequence of unique words periodically embedded in the transmitted symbol sequence. Beams with the

highest cross-correlation with the unique words are selected. In this thesis, we utilized the 10-period short training sequences of the 802.11a or 802.16a standard as the unique words. We also derived a simple method to represent the cross-correlation between received and original training sequences.

The PTR metric has three main advantages: (1) No channel state information (CSI) is needed, (2) data detection is not needed, and (3) the metric is robust to frequency-, time-, and sampling-offset. However, this metric cannot be used when interference is caused by users in the same system (the same training structure).

In this chapter, we describe the receiver system and propose the associated beam selection algorithm. We present experimental performance of the peak-to-trough (PTR) metric, which was evaluated with the Georgia Electronic Design Center (GEDC) high-speed link prototype in an indoor environment with uncorrelated interference. We also present the relationship between the PTR and SINR. The chapter also shows that the beam selection algorithm based on the PTR is robust to synchronization offsets for 802.11a and 802.16a waveforms. Simulated symbol error rate (SER) performance and experimental received OFDM waveforms are also presented.

3.2 System Structure

We apply this beam selection algorithm to a 2×2 MIMO system. The transmitter consists of two omnidirectional antennas. The switched-beam receiver system uses two selected beams. Two possible configurations for the receive antennas are as follows: (1) Two antenna arrays, each followed by a multi-beam beamformer; one beam is selected from each beamformer to form the two selected beams; (2) one antenna array followed by one multi-beam beamformer; an associated switch matrix chooses two of the beams. Configuration 2 has a simpler structure than configuration 1. But in configuration 2, one selected beam nearly always yields a lower average power than the other selected beam, leading to diminished diversity performance [33]. Therefore,

configuration 1 has the advantage that the two selected beams could both point in the same direction, and yield comparable average powers and uncorrelated fading [14]. In this chapter, we use configuration 2 to simplify our analysis and focus on selection metric performance. The two configurations are compared in Chapter IV.

The system schematic of the receiver, which implements the dual-metric beam selection algorithm [32], is shown in Figure 6. The micro-controller first arranges the beams based on RSSI. The sensors, which test each beam's strength, are on the switch matrix board. They send the measured RSSI to the controller immediately. The beams with the two highest RSSI are selected. Then, the second metric tests whether there is too much interference in the beams. If there is not much interference, the two selected beams will not change. Otherwise, one or two beam rejection signals are sent from the DSP to cause the rejected beam (or beams) to be replaced by the next strongest beam (or beams).

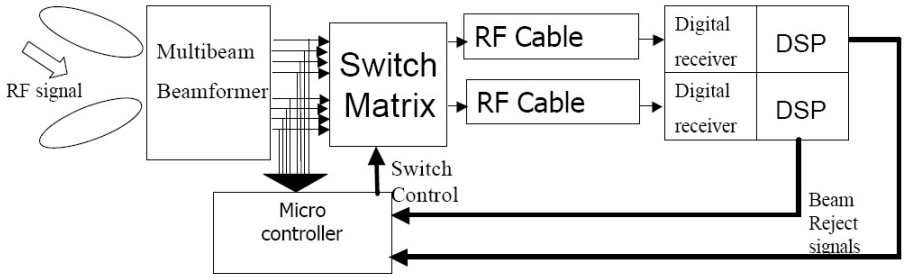

Figure 6: System schematic.

3.3 PTR Metric

In this section, we describe the PTR metric, which we use for the "second" metric, or the one implemented above in the DSP, as shown in Figure 6.

In the orthogonal frequency division multiplexing (OFDM) standards 802.11a [1] and 802.16a [2], training symbols are embedded into physical layer preambles as the unique words. The 802.11a and 802.16a OFDM waveforms have 10 and five periods

of short training symbols, respectively.

According to [32], we first arrange the beams in order of descending RSSI. Then, we check the beams' PTR values in order. If the PTR value is less than a threshold (which can be set based on a real system's requirement), we conclude that this beam has too much interference and noise; then we check the next strongest beam until we find a PTR value that is higher than the threshold.

To get the PTR value, we use the following equation:

$$R_x(m) = \frac{\left|\sum_{n=0}^{N1} \bar{r_x}(n+m)\bar{t_x}^*(n)\right|}{\left|\sum_{n=0}^{N1} \bar{r_x}(n+m)\bar{r_x}^*(n+m)\right|}, \quad (36)$$

$$m = 0, 1, 2....N2$$

where r_x is the received short training sequence, which includes noise and interference, and t_x is the original one-period-long training sequence. N1 is the length of one period of the training sequence (16 symbols for 802.11a and 64 symbols for 802.16a). N2 is the length of the whole short training sequence plus one period length (for 802.11a, it is $10 \times N1 + N1 = 176$, for 802.16a, it's $5 \times N1 + N1 = 384$). $R_x(m)$ is the normalized cross-correlation function. If the received signal includes limited noise and interference, $R_x(m)$ will have N2/N1-1 peaks. Then, each peak and some points on each side of it are removed. The remainder depends on the correlation of the training sequence with the noise and interference.

The PTR metric is computed as

$$PTR = \frac{< (\text{magnitude of the peaks})^2 >}{< (\text{magnitude of the remainder})^2 >}, \quad (37)$$

where <> indicates a time average.

Figures 7(a) and (b) show the results of an wired hardware test of the cross-correlation output $R_x(m)$ of the training sequences. The over-sampled 802.11a preamble was generated and has 64 samples for one period of the training sequence. The

output of a white noise generator, which represents both noise and uncorrelated interference, is added to the intermediate frequency (IF) signal through a power combiner before sampling. The PTR metric was computed in the digital receiver's DSP. Figure 7(a) is the result of the sliding correlation of the 802.11a preamble with one OFDM training symbol when the noise generator is off. The peaks and troughs of the correlation are clear. Figure 7(b) shows $R_x(m)$ when extra noise and interference are added, where the troughs are higher than in Figure 7(a)

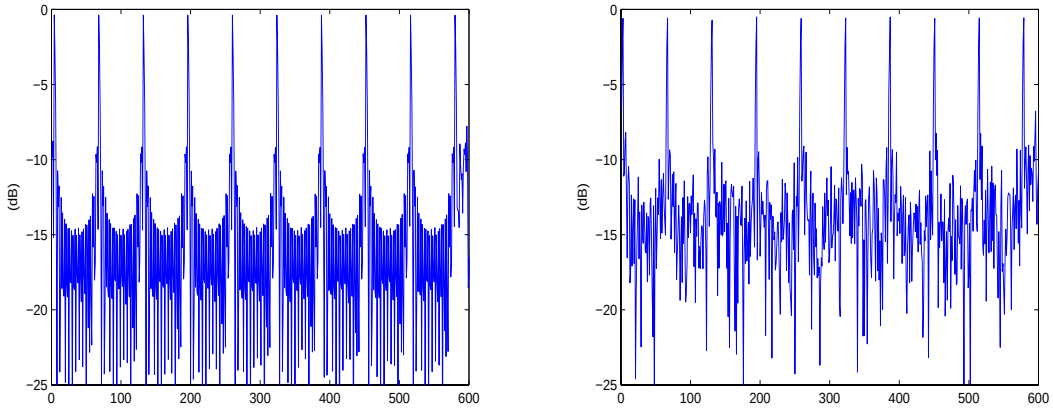

(a) Without interference and noise

(b) With interference and noise

Figure 7: The cross-correlation output $R_x(m)$.

Varying the amounts of additive noise and calculating the PTRs for 10 trials for each noise value, the sample values of the PTR metric for each noise power value are shown in Figure 8. An example beam reject threshold is shown. This figure shows that the PTR is an effective indicator of SINR.

3.4 PTR Metric's Synchronization Performance

Because the PTR beam selection algorithm operates directly on the IF signal, it has fast feedback ability and does not need more digital signal processing such as diversity combining, demodulation, and channel estimation. We also hope no synchronization

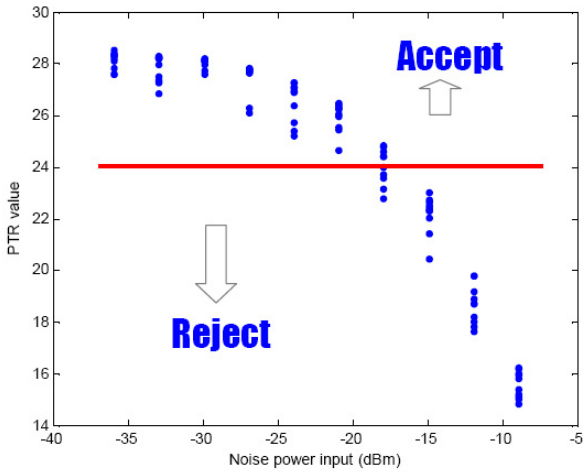

Figure 8: PTR with different noise.

will be performed before the PTR calculation. Otherwise, the feedback is delayed and the accuracy for beam selection in a time-varying channel, such as an indoor wireless environment, is degraded. Therefore, we should test whether the PTR metric is robust enough to the synchronization offsets: frequency offset, sampling frequency offset, and frame time offset. Another type of offset, carrier phase offset, obviously has no impact on the PTR metric from equations (36) and (37).

We will test the PTR metric for two wireless standards: 802.11a, which is the wireless LAN standard, and 802.16a, which is the fixed wireless access standard. The standards have different tolerances or maximum offsets.

For the 802.11a standard, the transmit center frequency tolerance is 20 parts per million (ppm) maximum, ($5\ GHz \times 20\ ppm = 100\ kHz$). The symbol clock frequency tolerance is 20 ppm maximum. About frame time offset, based on the algorithm of searching the beginning of a short training sequence, error within a 0.1 period is guaranteed. That is $0.8 \times 0.1 = 0.08\ \mu s$.

For 802.16a, we should notice that the carrier frequency is 2.4 GHz, and the frequency accuracy tolerance is +/-15 ppm maximum. So the frequency offset will be limited under $2.4\ GHz \times 15\ ppm = 36\ kHz$.

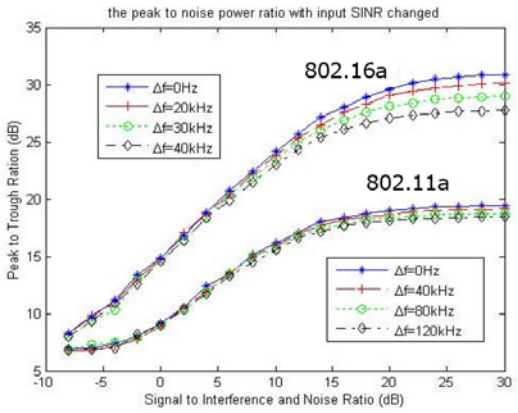

(a) PTR under Frequency offset

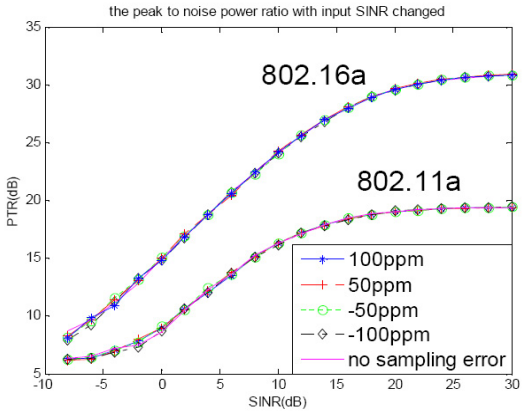

(b) PTR under sampling offset

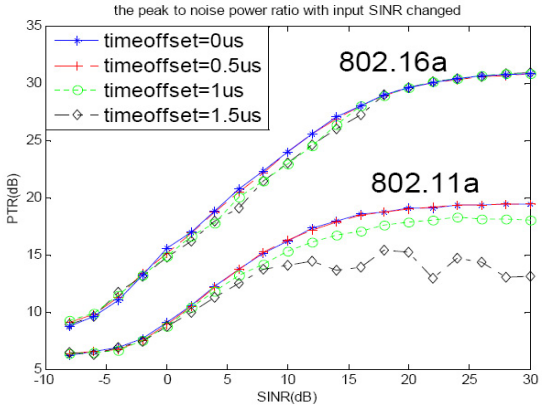

(c) PTR under frame time offset

Figure 9: Synchronization performance of PTR metric.

PTR versus SINR curves for different types of synchronization offsets are shown in Figures 9. Assuming that the interference is uncorrelated with the short training symbols, we observe that the PTR monotonically increases with SINR, with a nearly linear characteristic in the 0 to 15 dB range. Even when the synchronization offset is higher than the tolerance value in the standard, the curves are not changed much. In Figure 9 (a), the PTR curves are converge to different levels with different frequency offset values in the high SINR situation. The 802.16a standard is more sensitive with frequency offset. But there are no big changes when SINR is relatively low (0 to

15 dB), which means the PTR metric is robust to frequency offset if the rejection threshold is set to cross the linear part of the PTR curves. In Figure 9 (b), we find sampling offset has nearly no influence on the PTR curves. In Figure 9 (c), which shows the frame time offset influence, we choose a very large value ($1.5\ \mu s \gg 0.08\ \mu s$). So we can see an obvious degradation of the 802.11a curves when the SINR is above 10 dB. But this case will absolutely not occur. We can also observe, even with such high time offset value, that the PTR curves for 802.16a waveforms are still similar to each other. Because of the relatively low carrier 2.4 GHz, the PTR metric becomes more robust against the time offset. The limited changes of the curves with the synchronization offset values indicates the robustness of the PTR metric under offset conditions.

3.5 Simulation and Experimental Results

This section first introduces the simulated system diagram and then studies the SER performance of the two selection metrics: PTR and RSSI. Finally, the experimental received waveforms for selected beams and omnidirectional antenna are presented.

The system diagram is shown in Figure 10. Two omnidirectional antennas transmit independent data streams simultaneously. An interference source transmits uncorrelated interference (white Gaussian) from another direction. The positions of the data source (TX), interference source (I), and receiver array (RX) are shown in the low-right part of Figure 10. For simplicity, we consider that the RX conducts a 4-2 selection.

The channel data is measured in the Old Civil Engineering Building at Georgia Institute of Technology with the 3D MIMO channel measurement system [13]. During the channel data recording process, all the doors were open. The walls around the TX were wooden walls; the others were concrete walls.

All the antenna elements were at a height of 1.35 m. At the receiver (RX), a virtual

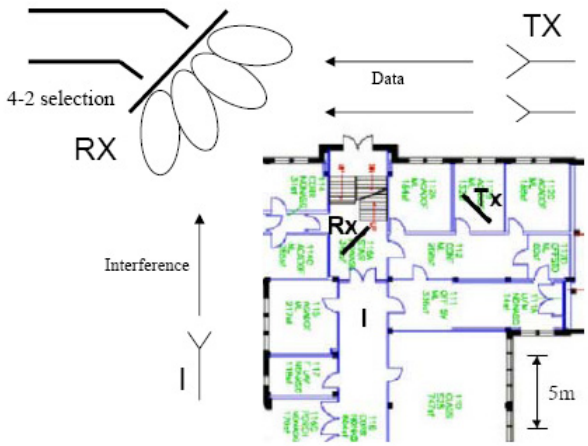

Figure 10: Simulation system diagram.

10-element uniform linear array (ULA) was formed using a biconical antenna, which was omnidirectional in azimuth. Only the first four-elements ULAs are considered for the digital beamformer, which is a 4×4 Butler matrix [39]. Similarly, the first two and one-elements ULA are chosen for the data source (TX) and interference source (I), respectively. The antenna spacing is 0.5λ, where λ is the wavelength of the 6.0 GHz signal. Fifty-one frequency samples within 6.0-6.5 GHz were chosen so that the separation between adjacent samples (10 MHz) is large enough to have a low correlation realization of flat-fading channels. As a consequence, for each TX-RX link, there are 51 realizations of flat-fading MIMO channels and, therefore, 51 independent samples of link SER. The measured MIMO channels are normalized with their mean value [14]. Therefore, path loss is not considered.

The simulations use the waveform structure of the 802.11a standard. Each OFDM symbol has 64 subcarriers, 52 of which are used to transmit data. Although 20 to 40 user data symbols can be included for each OFDM frame, one user data symbol per frame is enough for SER calculation. For each subcarrier of the OFDM symbol, the modulation method is QPSK. Zero forcing linear detection of the spatial multiplexing data streams is used for the receive data vectors on each subcarrier. Channel information is ideally estimated at the receivers. SER is averaged over all the 51 frequency

samples within 6.0-6.5 GHz.

Figure 11 shows the SER vs. SIR curves with different selection metrics, where MSER means selection based on the minimum SER and MMSV means selection based on the maximum minimum singular value of the channel matrix. SIR is defined as the value of the transmitted data source power divided by the transmitted interference power. The SNR at the output of each beam is 40 dB. We find that MSER is the optimal selection metric. Because of the time-consuming calculations, we can only apply practical metrics such as MMSV in real systems. In the high SIR situation, RSSI has similar performance as MMSV, while in the low SIR situation, because of the beam-falsing problem, RSSI becomes worse. The PTR metric fixes the beam-falsing problem very well in the low SIR situation. From Figure 9, we know that in the high SINR situation, the PTR curves are nearly flat, which means the lose of functionality as the indicator to SINR. Therefore, in Figure 11, we observe that the SER performance for the PTR metric is bad in the high SINR situation. Although the PTR metric has such a drawback, combining with RSSI, the SER performance is nearly the same as with the MMSV metric.

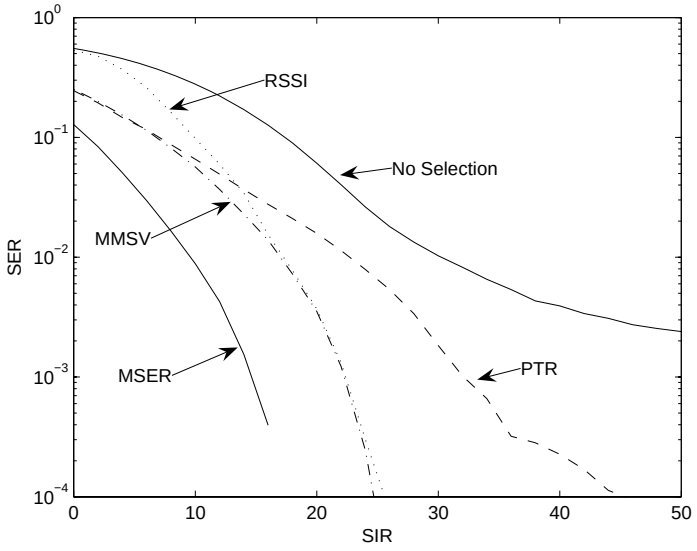

Figure 11: SER for different selection metrics with receiver's SNR=40 dB.

Figure 12 shows the same curves again when the SNR at the output of each beam is 30 dB. We find that with relatively lower SNR, the RSSI and PTR metrics can work efficiently only when the SIR is lower than 25 dB. With decreasing SNR, the RSSI and PTR metrics result in SER floors. We can conclude that the RSSI and PTR metrics are the better choice for high SNR or low SIR situation. While in the low SNR and high SIR situation, MMSV is the better choice, at the cost of channel estimation processing.

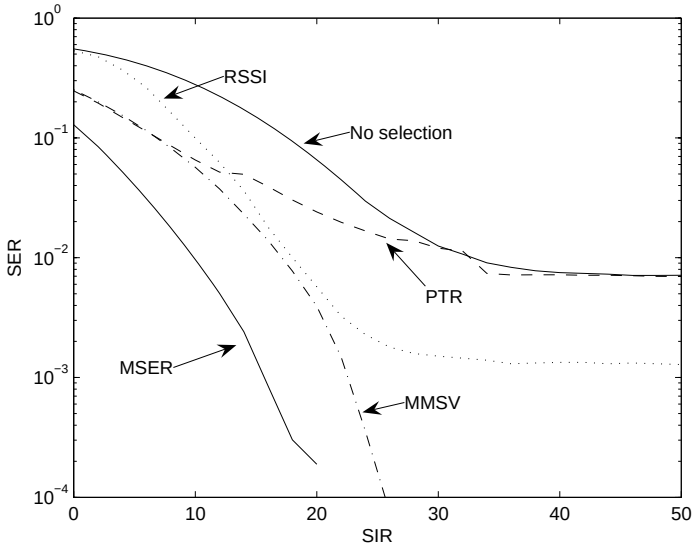

Figure 12: SER for different selection metrics with receiver's SNR=30 dB.

Our work also shows that the SER curves have no obvious difference if we choose thew 802.16a waveforms. Therefore, the results for 802.16a standard are not presented.

After running this dual-metric beam selection program in the GEDC testbed, where the system schematic of the receiver is shown in Figure 6, the interference can obviously be recognized and suppressed. Figure 13 shows the received OFDM waveforms, which are simultaneously recorded by an oscilloscope through an omnidirectional receive antenna and one selected beam of the receive antenna array. Burst interference signal is generated to make the interference easily indentifiable. We can

observe that the interference of the middle OFDM frame is strong for the omnidirectional antenna, while the interference is strongly suppressed for the selected beam.

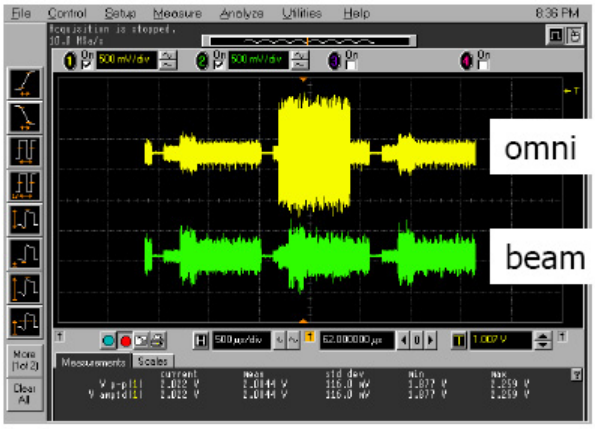

Figure 13: Interference suppression with one selected beam.

3.6 Conclusion

This chapter describes our multi-beam receive system and the principle of the PTR metric beam selection algorithm. Combined with RSSI selection, the PTR metric will select beams that have both good desired signal gain and little probability of including large noise and interference.

Through analysis and simulation, we found that the PTR metric is robust to synchronization offsets for 802.11a and 802.16a waveforms. The dual-metric (RSSI and PTR) selection method is a good choice for systems with high SNR or low SIR.

CHAPTER IV

MIMO RECEIVER SELECTION ARCHITECTURES FOR MEASURED INDOOR MIMO-OFDM CHANNELS

In this chapter, we compare the performance of low-complexity antenna and beam subset selection methods for small multi-user MIMO networks with non-distributed and spatially distributed access points. We show the advantages that beam selection can give over antenna selection and that a distributed access point can give over a non-distributed access point in some indoor environments. The simulation results show that these advantages are related to the channel correlation at the receivers, the signal angle spread, and the multi-beam receiver's beamwidth. Explanations are given for these results and a new MIMO selection strategy for indoor channels is proposed. We also compare three selection criteria: minimum symbol error rate (MSER), maximum channel capacity (MCC), and the maximum of the minimum singular value (MMSV) of the MIMO channels. Simulations use 802.11a OFDM waveforms with ideal channel estimation [1], where the same selection is made for every subcarrier. Two scenarios of network type (2) with high and low correlation coefficients are considered.

4.1 MIMO Channel Measurement System and the Measured Indoor Channel

The 3D MIMO channel measurement system is illustrated in Figure 14 and is the same as in [28]. The MIMO channel measurement system is composed of two parts: (1) the HP 85301B stepped-frequency antenna pattern measurement system, which, because of its coherent reference signal, can measure the channel frequency response directly, and (2) the actuator positioning system, which creates the virtual array by moving the antenna to arbitrary pre-programmed locations.

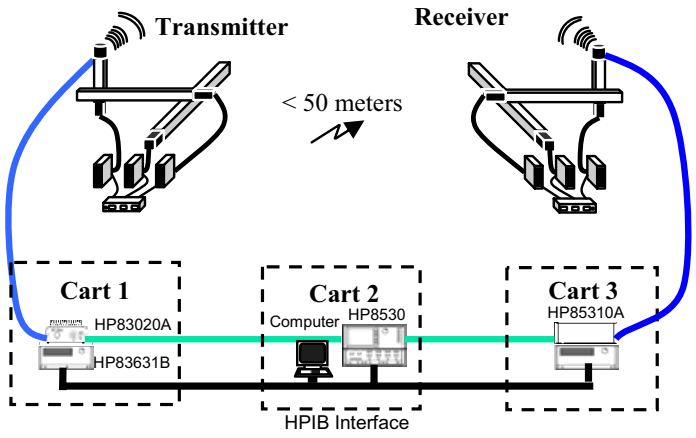

Figure 14: MIMO channel measurement system.

The measurements are conducted in the Old Civil Engineering Building at Georgia Institute of Technology. Figure 15 shows the locations of three transmit arrays (TX) and five receive arrays (RX). The line on each position represents the arrangement of the linear array.

The TX and RX antennas were both at a height of 1.35 m. At each node, a virtual 10-element uniform linear array (ULA) was formed using a biconical antenna, which was omnidirectional in azimuth. All 10 elements were used for normalization; however, only the first eight- or four-element ULAs are considered for the digital beamformers. The antenna spacing is 0.5λ, where λ is the wavelength of a 6.0 GHz signal. Fifty-one frequency samples within 6.0-6.5 GHz were chosen so that the separation between adjacent samples (10 MHz) is large enough to have a low-correlation realization of flat-fading channels. As a consequence, for each TX-RX link, there are 51 realizations of flat-fading MIMO channels and, therefore, 51 independent samples of link SER. With three TX and five RX, there are 15 MIMO links.

During the channel data recording process, all the doors shown in Figure 15 were open. The walls around T3 and R5 were wooden walls; the others were concrete walls. We can observe that the receivers R3 and R5 were in the hallway. Links T2-R3 and T3-R5 had line-of-sight (LOS) paths. Because of the open doors and wooden

Figure 15: Layout of old Civil Engineering Building.

walls, links T2-R5 and T3-R3 had a narrow angle of arrival (AOA). Therefore, all the previous four links possess a strong cluster. Receiver R1 was in an empty classroom. The main signal energy came in through the door, plus a few one-time wall-bounced paths, so links T1-R1 and T2-R1 had wide AOA with main signal power directional, which means a few strong clusters. Receiver R2 was in an equipped restroom, which brought the rich scattering characteristic. Links T1-R2 and T2-R2 can be considered as nearly i.i.d channels.

4.2 The Access Point Architectures

Two access point architectures are used for simulation, which are distributed receivers and a non-distributed receiver, respectively.

The system model of distributed receivers is shown in Figure 16(a). There are two users, where each user transmits two independent data streams. The access

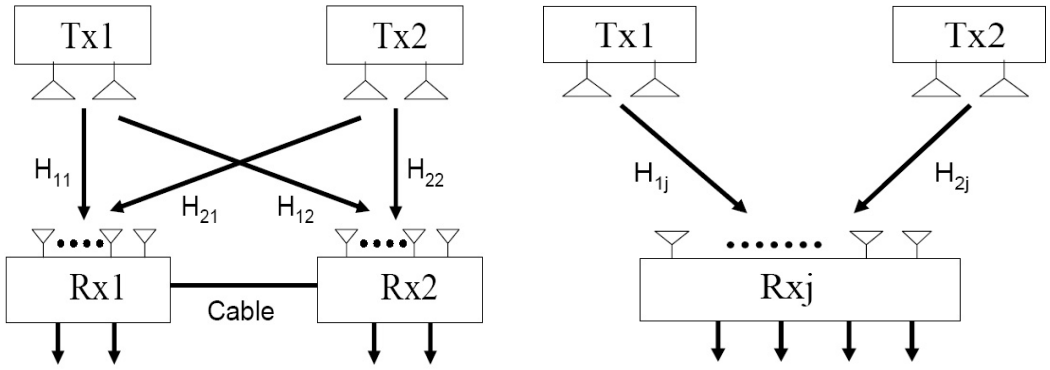

(a) Distributed receivers (b) A non-distributed receiver

Figure 16: Multiuser MIMO selection system with non-distributed or distributed receivers.

point is distributed with two receivers, which are normally in two different rooms or far enough away to acquire a both macroscopic and microscopic spatial-diversity benefit. A simple four-node network with any two TX and two RX chosen from Figure 15 is considered. Each TX node (TX1, TX2) uses the first two antennas of its linear array, while each RX node (RX1, RX2) chooses two antennas or beams from a total of either four (4-2 selection) or six (6-2 selection) antennas or beams. The selection for RX1 and RX2 is done jointly. A combined 4×4 MIMO link is created to evaluate the SER performance after such selection.

The system model of a non-distributed receiver is shown in Figure 16(b). The access point is one receiver with an eight-element antenna array; the position can be any RX in Figure 15. All four antennas or beams are chosen from the total of eight antennas or beams. So, after selection, both the non-distributed and distributed receivers result in a 4×4 MIMO channel.

We next discuss two different ways we will normalize these channels. The normalization is calculated for MIMO networks with distributed receivers. Such normalization is easy to extend to MIMO networks with a non-distributed receiver.

We first discuss the distance preserving normalization. With the choice of any

two TX and two RX, we have four links total (TX1-RX1, TX1-RX2, TX2-RX1, TX2-RX2). For each frequency sample k, each link TXi-RXj's raw channel data is a 10×10 matrix $\hat{H}_{ij}^k$, where $i, j = 1, 2$ and $k = 1...51$. We assume the combined channel for all four links is $\hat{H}^k$. It is easy to see that $\hat{H}^k$ is a 20×20 matrix. So the normalized channel matrix H_{ij}^k is calculated as

$$H_{ij}^k = \frac{\sqrt{51 \times 20 \times 20} \times \hat{H}_{ij}^k}{\sqrt{\sum_{k=1}^{51} \parallel \hat{H}^k \parallel_F^2}}, \tag{38}$$

where $\parallel \cdot \parallel_F$ means the Frobenius norm. The normalization makes the average magnitude square value of each element approximately 1. Because this normalization keeps the *relative* distance and path loss information of each TXi-RXj link, we call it the distance preserving normalization.

Most MIMO researchers assume equal variance for each entry, which provides the motivation for another normalization. The method is to normalize each TXi-RXj link first and then combine all four links together. Because it removes the path loss information and keeps the average square value of each link equal to each other, we call it the equal SNR normalization, which is calculated as

$$H_{ij}^k = \frac{\sqrt{51 \times 10 \times 10} \times \hat{H}_{ij}^k}{\sqrt{\sum_{k=1}^{51} \parallel \hat{H}_{ij}^k \parallel_F^2}}. \tag{39}$$

The mathematical expressions for antenna and beam selection are similar to [29]. N_T and N_R denote the numbers of transmit and receive antennas, respectively. n_T and n_R denote the numbers of selected transmit and receive antennas, respectively. The measured normalized channel matrix for link TXi-RXj, denoted as H_{ij}, is an $N_R \times N_T$ matrix. For the considered network, $N_T = n_T = 2$ for each transmit antenna (TX1, TX2). To form the 4×4 MIMO channel, two antennas or beams are selected at each receiver (RX1, RX2), which means $n_R = 2$. The $n_R \times n_T$ MIMO channel matrix for link TXi-RXj after antenna selection and beam selection is given

by

$$H_{ij}^{ant} = J_R H_{ij} \tag{40}$$

$$H_{ij}^{beam} = J_R B_R H_{ij} \tag{41}$$

respectively, where $J_R \in \boldsymbol{R}_{n_R \times N_R}$ is the lossless receive selection matrix, $B_R = [B_R^1\ B_R^2 \cdot \cdot \cdot B_R^{N_R}] \in \boldsymbol{C}_{N_R \times N_R}$ is the lossless receive Butler matrix [39]. The m^{th} column of B_R is

$$B_R^m(n) = \frac{1}{\sqrt{N_R}} e^{\frac{j\pi(m-1)[-(N_R-1)+2(n-1)]}{N_R}}, n = 1 \cdots N_R \tag{42}$$

For the 4-2 beam selection, the first four elements of each receive array are connected to the 4×4 receiver Butler matrix to form four receive beams, which can cover about 110^o on each side of the array. For the 6-2 beam selection, the first eight elements of each receive array are connected to the 8×8 receiver Butler matrix to form eight receive beams. Because of the wide and low beam patterns [39], the two outside beams are abandoned; the remaining six middle beams can cover 90^o on each side of the array. Two beams are selected from those remaining six.

The combined 4×4 MIMO channel matrix for a four-node network after antenna and beam selection is given by

$$H^{ant} = \begin{bmatrix} H_{11}^{ant} & H_{21}^{ant} \\ H_{12}^{ant} & H_{22}^{ant} \end{bmatrix},\ H^{beam} = \begin{bmatrix} H_{11}^{beam} & H_{21}^{beam} \\ H_{12}^{beam} & H_{22}^{beam} \end{bmatrix}. \tag{43}$$

For the non-distributed access point in Figure 16(b), all four antennas or beams are selected from the eight-element array at either RX1 or RX2. According to the mathematical expressions above, we can easily find $n_R = 4$. The combined 4×4 MIMO link after antenna and beam selection can be expressed as $H^{ant} = [H_{1j}^{ant}\ H_{2j}^{ant}]$ and $H^{beam} = [H_{1j}^{beam}\ H_{2j}^{beam}]$, where $j = 1, 2$. One goal of this research is to compare the non-distributed receiver with distributed receivers, where only 4-2 selection is conducted for each receiver of the distributed access point. In this case, a total 8-4 selection is conducted for either a non-distributed or distributed access point.

The optimal selection criterion is the minimum SER (MSER). However, the MSER is not a practical criterion because the calculation is time consuming. So real systems would use a practical selection criterion [12]. In this paper, two practical selection criteria are considered. The first one is the maximum channel capacity (MCC), which is calculated according to the following equation [16]:

$$C = log_2 \mid I + \frac{\rho}{n_T} H H^H \mid, \tag{44}$$

where ρ is the signal-to-noise ratio per antenna at the receiver. Antenna or beam selection should let the channel matrix H^{ant} or H^{beam} have the maximum channel capacity.

The second practical selection criterion is the maximum minimum singular value (MMSV) of the channel matrix. From [25], with the ZF linear receiver, the minimum post-processing SNR_{min} is lower-bounded by λ^2_{min}. Therefore, antenna or beam selection can choose the channel matrix H^{ant} or H^{beam} with the MMSV to increase the SER performance.

Although the MSER is not a practical criterion, its SER curve can be used as the low bound of the other two criteria. Depending on the gap between the optimal selection criterion and practical ones, we know the space left for better practical selection criterion design.

4.3 Simulation Results

This section first analyzes the difference between antenna and beam selection and then studies the difference between non-distributed receiver and distributed receivers.

4.3.1 Comparison of Antenna and Beam Selection

We consider the dual-user and distributed dual-receiver scenarios. The transmitters and receivers selected from Figure 15 are (T2, R3, T3, R5) and (T1, R1, T2, R2)

respectively. We call the first Scenario I and the second Scenario II. Only the distance preserving normalization is considered in this subsection.

Figure 17 shows the correlation coefficients at the receiver for every link of the two scenarios. We can see that Scenario I has a higher correlation than Scenario II. After looking at Figure 15 carefully, we can easily see that Scenario I has the LOS channel links or the narrow AOA links, which were described in Section 4.1. For example, the Rice factor $K = 1.7622$ for link T2-R3, while $K = 1.2762 \times 10^{-7}$ for link T1-R2, where K is calculated using MATLAB Distribution Fitting Tool. So, it is reasonable to observe the large correlation difference between these two scenarios [42].

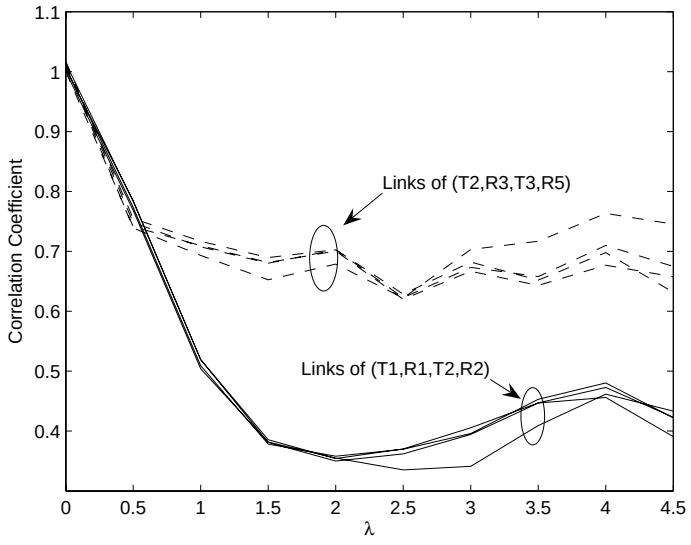

Figure 17: Receiver correlations for Scenario I (T2, R3, T3, R5): (dashed curves) and Scenario II (T1, R1, T2, R2): (solid curves).

The simulations use the waveform structure of the 802.11a standard. Each OFDM symbol has 64 subcarriers, 52 of which are used to transmit data. Although 20 to 40 user data symbols can be included for each OFDM frame, one user data symbol per frame is enough for SER calculation. For each subcarrier of the OFDM symbol, the modulation method is 64-QAM. Zero-forcing linear detection of the spatial multiplexing data streams is used for the receive data vectors on each subcarrier.

Channel information is ideally estimated at the receivers. SER is averaged over all 51 frequency samples within 6.0-6.5 GHz. In all the following figures, "AS" represents antenna selection; "BS" represents beam selection; and "NS" represents no selection (for m-n selection case, the first n antennas are chosen).

We expect beam selection to have no obvious difference from antenna selection in i.i.d channels. This is because the beamformer is only a normalized phase shift matrix, which does not change the statistics properties of i.i.d channels. This characteristic was is demonstrated in Figure 18.

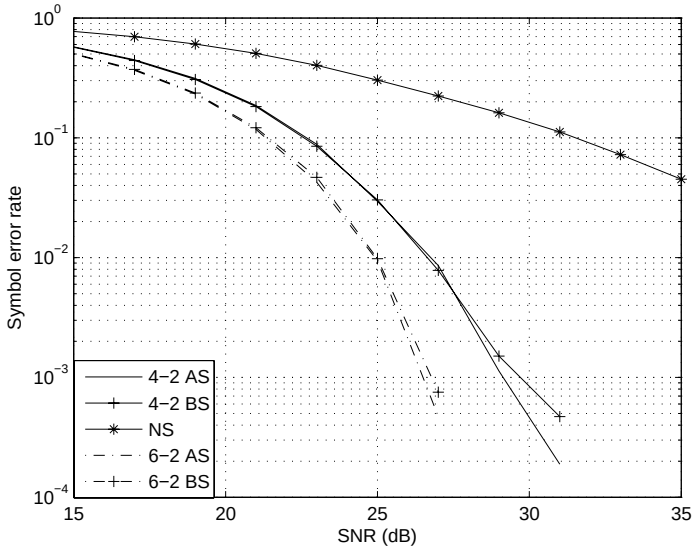

Figure 18: SER over i.i.d channel.

Figure 19(a) and (b) show the SER performance with the measured channels for Scenarios I and II, respectively. To simulate real wireless environments, the distance preserving normalization is used to keep the relative path loss differences between all the MIMO links. From Figure 17, we already know Scenario I has the higher correlation. We observe that in Figure 19(a), beam selection offers a greater improvement over antenna selection. For example, at $SER = 10^{-3}$, beam selection offers almost 5 dB over antenna selection for the 6-2 selection and 3 dB for the 4-2 selection, while in

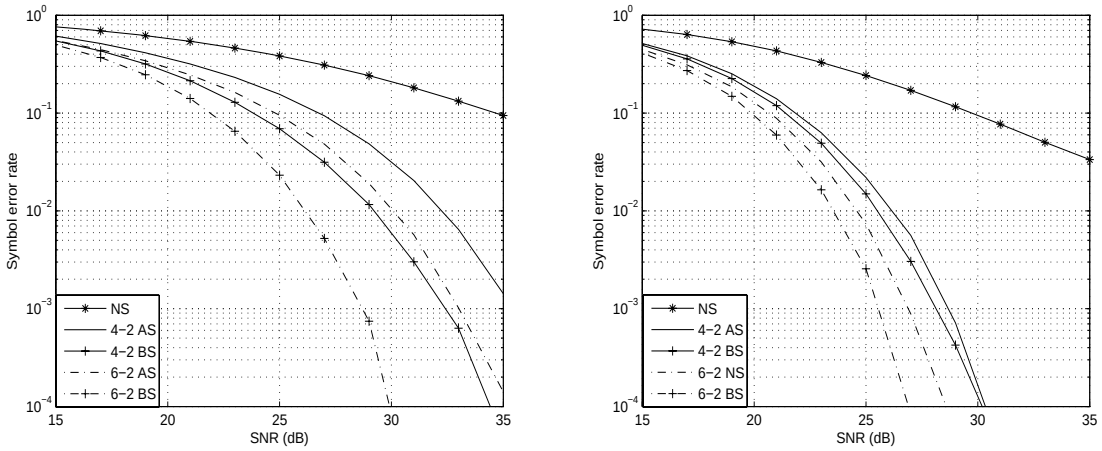

(a) high-correlated Scenario I (T2, R3, T3, R5)

(b) low-correlated Scenario II (T1, R1, T2, R2)

Figure 19: SER performance with the distance preserving normalization.

Figure 19(b), beam selection only offers $1 \sim 2$ dB over antenna selection. These results match [36] very well. However, the authors in [36] consider a geometric outdoor channel model [46], which is not suitable for indoor applications like a 802.11 MIMO-OFDM system. It also does not consider the SER performance, which is mostly of interest for engineering. Simulations in [42] show that the BER increases with decreasing AOA. Comparing Figure 19(a) and (b), we find that Scenario II has lower SER than Scenario I. The results match [42], because we already know the receivers in Scenario I have the narrower AOA spread than the receivers in Scenario II. We also find, in Scenario I, that the 6-2 *antenna* selection is only a little bit worse than the 4-2 *beam* selection, while in Scenario II, the 6-2 antenna selection is better than the 4-2 beam selection. This is because in the low-correlation scenario, antenna selection has more diversity gain. So, for the indoor channels, we do not prefer the 4-2 beam selection method, because a 4×4 beamformer is more complex than an additional two antennas.

Figure 20 compares selection criteria over Scenario I. Beam selection curves are

all dash-dot and antenna selection curves are all solid. Only the 6-2 selection is considered to make the figure easy to read. We can see that MSER is the optimal selection criterion. Although [5] tells us there is only limited degradation in the i.i.d channel, this figure tell us there is a large performance degradation of the two practical criteria (MCC and MMSV) compared with the optimum one (MSER) in this set of measured indoor channels. So, work on designing better practical criteria is still needed. We also find in these high-correlated channels that the MCC criterion is a little bit better than the MMSV criterion, while in the low-correlated channels (Scenario II), our simulations (not present because of space constraints) show that there are no obvious differences between the two criteria.

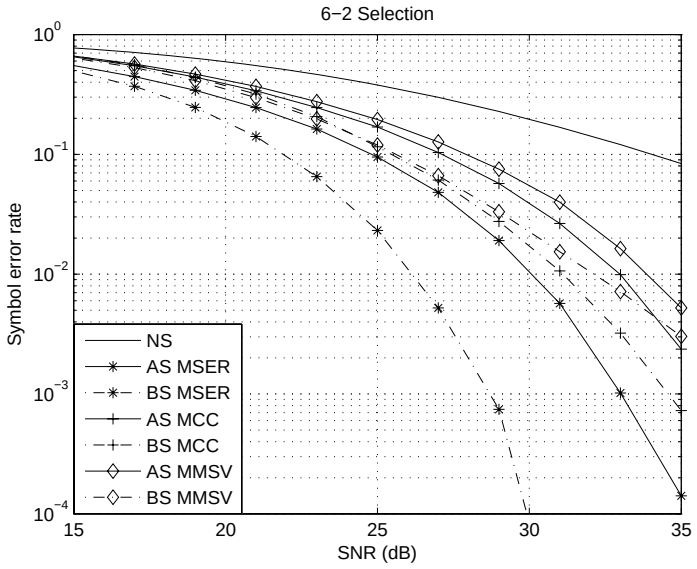

Figure 20: SER over high-correlated Scenario I (T2, R3, T3, R5) with three different selection criteria.

4.3.2 Comparison of Non-distributed and Distributed Receivers

In the previous section, we considered distributed receivers with the distance preserving normalization. In this section, we compare the non-distributed and distributed receivers, with both the distance preserving normalization and equal SNR normalization.

To conduct a fair comparison, we should assume that the total antenna elements are the same. So, both the non-distributed and distributed receivers use the total 8-4 selection, which was discussed in Section 4.2. For distributed receivers, two antennas or beams are selected at each of the four-element arrays. For a non-distributed receiver, all four antennas or beams are selected from the eight-element array at one receiver position. We should note that, when beam selection is conducted, we have eight narrow beams (8×8 butler matrix) for the non-distributed receiver, but four wide beams (4×4 butler matrix) for each of the two distributed receivers. So, the differences between the non-distributed and distributed receivers for beam selection are caused by both space diversity and angle diversity [31].

We already know, for the distance preserving normalization in the previous section, that beam selection gives a high performance gain over antenna selection in the high-correlated indoor channels. Sometimes, one non-distributed receiver has a better position than the other. For example, in Figure 15, we can observe that R5 has a better position than R3, when the two transmitters are T2 and T3. The reason is that R5 is nearly on the line between T2 and T3. So, compared with R3, the total distances from R5 to T2 and T3 are shorter, which brings the lower path loss. Simulated SER results in Figure 21(b) show that the non-distributed receiver R5 is even better than the distributed receivers R3 and R5 when choosing the distance preserving normalization. But we cannot say a non-distributed receiver is better than distributed receivers, just because this non-distributed receiver (R5) has a good position. When choosing the equal SNR normalization, which assumes each link has the same path loss, our simulated SER results in Figure 22 show that the distributed receivers R3 and R5 are better than either the non-distributed receiver R3 or R5.

Normally, the performance improvement in a system is defined by the improvement in the worst case. Therefore, we analyze and focus on the SER performance of the non-distributed receiver R3 and the distributed receivers R3 and R5. Figures

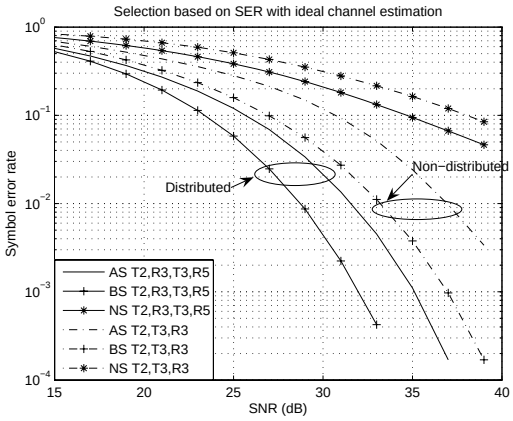

(a) The distributed receivers (R3,R5) vs. the non-distributed receiver R3

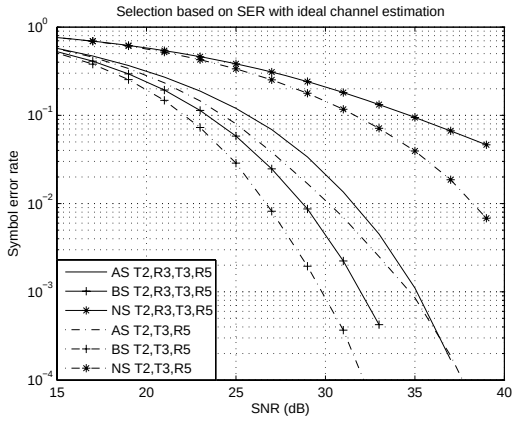

(b) The distributed receivers (R3,R5) vs. the non-distributed receiver R5

Figure 21: Distance preserving normalization with the transmitters T2 and T3.

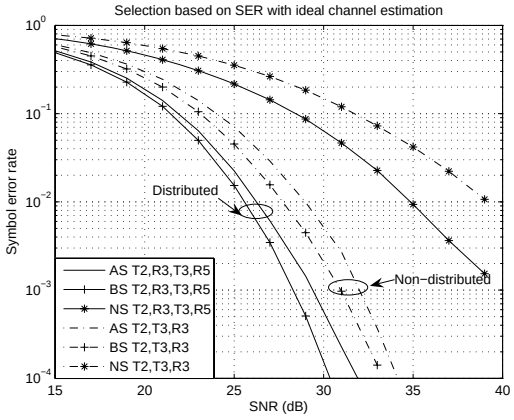

(a) The distributed receivers (R3,R5) vs. the non-distributed receiver R3

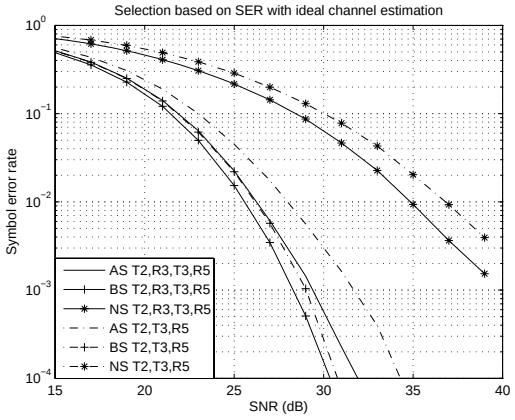

(b) The distributed receivers (R3,R5) vs. the non-distributed receiver R5

Figure 22: Equal SNR normalization with the transmitters T2 and T3.

21(a) and 22(a) give the results for Scenario I (high-correlated channels) with the distance preserving and equal SNR normalization, respectively. We find when we use the distributed receivers (T2 and T3 are the transmitters, R3 and R5 compose the distributed receivers) that the SER performance with selection is better than the non-distributed receiver (T2 and T3 are the transmitters, R3 is the receiver). Comparing Figures 21(a) and 22(a), we can see the trends are similar, except that all selection curves are closer in the equal SNR normalization case. This result can be explained as follows. The distributed receivers have different shadowing, and therefore the distributed architecture has a macroscopic diversity benefit. However, under the equal SNR normalization, the shadowing differences are normalized, so the distributed architecture yields less of a benefit. We also can see that Figure 21(a) has a worse SER performance than Figure 22(a). This is because the shadowing effect (the distance preserving normalization) is a dominating factor for capacity degradation [27]. Considering all the results of Figures 21(a) and 22(a), we can conclude that in the high-correlated indoor channels, such as an airport concourse or warehouse, beam selection with distributed receivers is the best choice. The normal feature of such channels is that they have one stronger cluster than others.

Instead of the high-correlated channels, we now consider the low-correlated channels (T1, R1, T2, R2), Scenario II. Because the TX and RX positions in Scenario II are like the four corners of a square, where each link has similar distance or path loss, the distance preserving normalization results are similar to the equal SNR normalization results. Figures 23 and 24 give the SER curves with the distance preserving and equal SNR normalization. We can observe that there is no big difference between them. Therefore, we choose the distance preserving normalization to analyze these low-correlated channels.

Although all four links to R1 or R2 are the low-correlated channels, there is still a difference between the environments around R1 and R2. We know R1 is in an

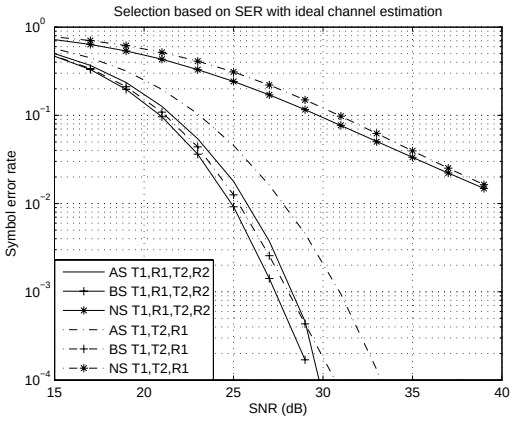

(a) The distributed receivers (R1,R2) vs. the non-distributed receiver R1

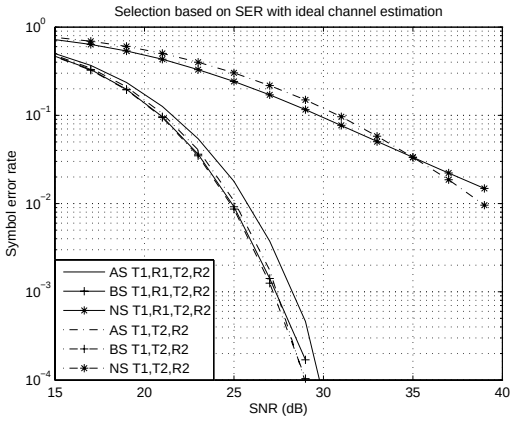

(b) The distributed receivers (R1,R2) vs. the non-distributed receiver R2

Figure 23: Distance preserving normalization with the transmitters T1 and T2.

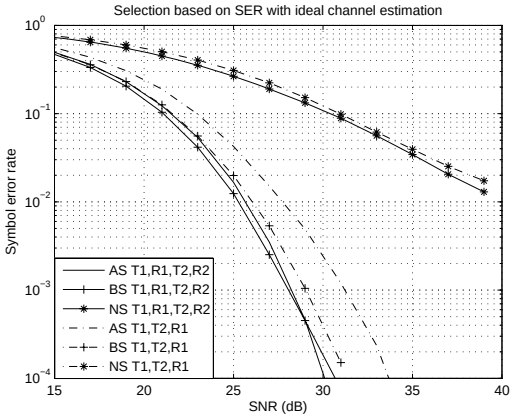

(a) The distributed receivers (R1,R2) vs. the non-distributed receiver R1

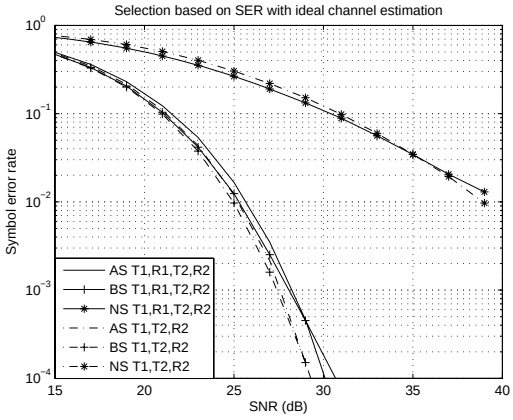

(b) The distributed receivers (R1,R2) vs. the non-distributed receiver R2

Figure 24: Equal SNR normalization with the transmitters T1 and T2.

empty classroom with an open door, which has a relatively wider AOA than Scenario I. Because of the reflection of walls, such channels have a few strong clusters. R2 is in an equipped restroom. The scattering source's structure is more complex than environments around R1. So, links to R2 are rich scattering, which are nearly i.i.d channels.

Let us first focus on Figure 23(a), which has the SER curves for distributed receivers R1 and R2 compared with the non-distributed receiver R1. We can see the non-distributed receiver with beam selection has a performance similar to that of the distributed receivers with either antenna selection or beam selection, and all of them have better performance gain (about 3 dB) over the non-distributed receiver with antenna selection. From [41], we know angle diversity offers a higher gain in low-correlated channels than in high-correlated channels. We also know that the angular spread is larger for Scenario II than Scenario I because of the lower correlation [42]. Results in [31] show that the narrow beams give higher angle diversity gain and less signal fading than the wide beams in the large angle spread channels. From this previous knowledge, we conclude that the four wide beams of each of the distributed receivers R1 and R2 have less angle diversity gain than the eight narrow beams of the non-distributed receiver R1. Although the distributed receivers supply an extra macroscopic diversity gain, for beam selection, the large part of this advantage is counteracted by the loss of angle diversity. Also, compared with high-correlated channels, the macroscopic diversity benefits are lower in low-correlated channels [4]. Therefore, for beam selection, the distributed receivers R1 and R2 have similar SER performance as the non-distributed receiver R1. From the previous section, we also know that, in Scenario II (low-correlated channels with the distributed receivers R1 and R2), beam selection has no major difference with antenna selection. Those facts explain the three close SER curves in Figure 23(a). On the other hand, for the non-distributed receiver R1, because of the few strong clusters and narrow beams (8-4

selection), beam selection offers a considerable gain over antenna selection. But, such gain is not as high as in Scenario I (high-correlated channels), which is shown in Figure 21(a).

We know beam selection with distributed receivers is the most complex architecture. So, with the observations from Figure 23(a), we can conclude that for the large angle of arrival channels with a few strong clusters, such as buildings with large conference rooms or classrooms, beam selection with a non-distributed receiver or antenna selection with distributed receivers is the better choice. Which one to choose depends on the complexity of the real implementation.

Figure 23(b), which has the SER curves for the distributed receivers R1 and R2 compared with the non-distributed receiver R2, demonstrates that for the nearly i.i.d channel, such as an office or home environment, there are no big differences for not only antenna and beam selection, but also the non-distributed and distributed receivers. So antenna selection with a non-distributed receiver is good and simple enough to implement.

With the simulations results above, we propose a new selection architecture guide for MIMO indoor channels. The guide is based on both system complexity and SER performance.

MIMO Selection Architecture Guide

- Beam selection with distributed receivers is the choice for high-correlation channels with one strong cluster (Figure 21(a)).
- Beam selection with a non-distributed receiver or antenna selection with distributed receivers is the choice for low-correlation but wide angle spread channels with a few strong clusters (Figure 23(a)).
- Antenna selection with a non-distributed receiver is the choice for rich scattering (nearly i.i.d) channels (Figure 23(b)).

4.4 Conclusion

In this chapter, we compare multi-user MIMO systems with selection over a set of measured indoor wireless channels. We analyze the SER performance improvement caused by the joint selection with some popular selection criteria. There is a significant SER gap between the optimal selection criterion (MSER) and both the MCC and the MMSV selection criteria for the high-correlated measured indoor channels, suggesting that improved sub-optimal selection criteria might be possible for this type of channel. Beam selection gives different gains over antenna selection in different indoor environments. The correlation level is the main reason for this difference. We also compare the non-distributed and distributed receivers. We observe that distributed receivers give an extra macroscopic diversity gain over a non-distributed receiver in the high-correlated channels. In the low-correlated channels with a few strong clusters, we can improve SER performance by either using distributed receivers with antenna selection or adding a beamformer at a non-distributed receiver to conduct beam selection. With these observations, a new MIMO selection architecture guide, considering both the system complexity and the SER performance, is proposed.

CHAPTER V

MIMO CHANNEL MODELING AND BEAMFORMER DESIGN

Three different MIMO channel models, the Kronecker model, the virtual channel representation and the Weichselberger model, were introduced in Section 2.6.

In this chapter, the Kronecker model, the virtual channel representation and the Weichselberger model are validated with our measured channel data. A new beamformer is designed based on the ideal of the Weichselberger model. The beam selection performance with the new beamformer is compared to the Butler matrix and the optimal beamformer.

5.1 MIMO Channel Model Validation

The locations of transmit arrays (TX) and receive arrays (RX) in the Old Civil Engineering Building are shown again in Figure 25(a). With three TX and five RX, there are 15 MIMO links.

In Figure 25(b), we compare three different models. The figure shows the models' channel capacity versus the measured channel capacity for each of the 15 links by means of a scatter plot. Equal SNR normalization, which was introduced in the previous chapter, is used for each link. Each data point in the figure corresponds to a specific model and a specific link. The channel capacity estimation is more accurate for a specific model and link if the corresponding point is closer to the identity line (dashed). Obviously, the Kronecker model underestimates the mutual information and the virtual channel representation tends to overestimate. The Weichselberger model shows a rather good match between measured and modeled channel capacity.

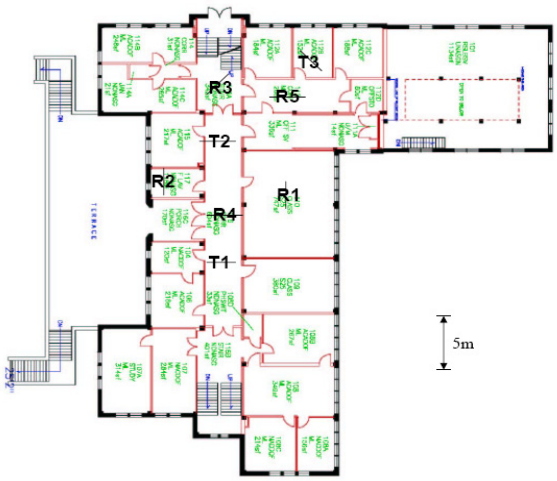

(a) Layout of old Civil Engineering Building

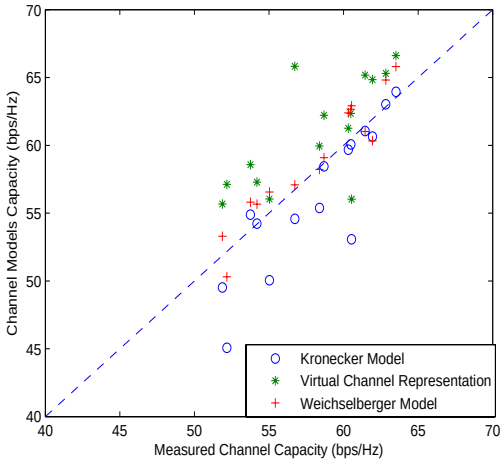

(b) Channel Capacity for each of the 15 measured indoor scenarios according to three different MIMO channel models versus measured mutual capacity

Figure 25: Layout of old Civil Engineering Building and capacity of 15 links.

This result matches the result in [47], which is obtained in different indoor measurements.

To further analyze the three channel models, we separate the 15 links into four different groups based on different indoor scenarios. Table 1 shows the links' order number and their related links.

From Figure 25(a), the first four links (Group 1) have line-of-sight (LOS) paths. Links 5,6,7 (Group 2) are the high-correlated channels without LOS paths. Links

Table 1: Link number vs. links.

Group 1		Group 2		Group 3		Group 4	
Number	Link	Number	Link	Number	Link	Number	Link
1	T1-R4	5	T2-R5	8	T1-R1	12	T3-R1
2	T2-R4	6	T3-R5	9	T1-R2	13	T3-R2
3	T2-R3	7	T3-R3	10	T2-R1	14	T3-R4
4	T1-R3			11	T2-R2	15	T1-R5

8,9,10,11 (Group 3) are the low-correlated channels. Links 12,13,14,15 (Group 4) are the remaining links, which have a long distance between transmitter and receiver. Because of the equal SNR normalization, the path loss difference between each link is not considered. Therefore, links in Group 4 can also be considered low-correlated channels.

Figures 26(a) shows the channel capacity of the three models and the measured channel for 15 measured indoor scenarios. We can see that the capacity of the Kronecker model and the virtual channel representation have a big difference compared to the capacity of the measured channel when the MIMO link has line-of-sight path. Figure 26(b) shows the variance of the capacity values in Figure 26(a). We can see that the first three links have a greater variance than the others. Although link 4 (T1-R3) belongs to Group 1, the long distance between transmitter and receiver brings more reflection. Therefore, link 4 has lower variance than the first three links.

Through the above analysis, we can conclude that, in line-of-sight MIMO scenarios, the Weichselberger model is much better than the Kronecker model and the virtual channel representation. In other cases, the Weichselberger model is slightly better than the Kronecker model and the virtual channel representation.

5.2 Beamformer Design

In Chapter IV, we compared beam and antenna selection in different indoor scenarios. The Butler matrix, which is the same as the DFT matrix in the virtual channel representation model, is chosen as the fixed beamformer at each receiver array.

This section investigates the following questions. How much improvement can we get with a novel beamformer design? What is the performance gap between the practical and optimal beamformer for a given environment?

From Section 2.3, we know that if channel information is known to the transmitter, considering the singular value decomposition of channel matrix $\mathbf{H} = \mathbf{U}\mathbf{\Sigma}\mathbf{V}^H$, the

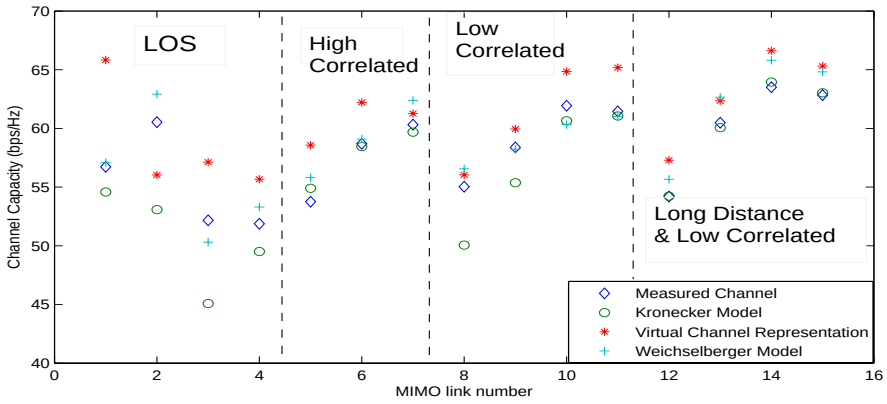

(a) Channel Capacity of three models and measured channels

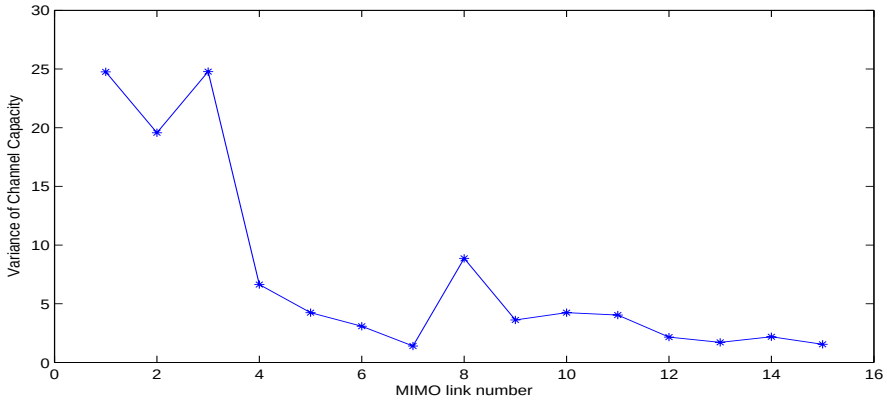

(b) Variance of Channel Capacity of three models and measured channels

Figure 26: Comparison of three models and measured channels for 15 measured indoor.

input-output relation for such a MIMO channel can be expressed as $\mathbf{y} = \sqrt{\frac{E_s}{N_T}}\mathbf{U\Sigma V}^H\mathbf{s}+\mathbf{n}$. Therefore, $\mathbf{H}$ can be explicitly decomposed into r parallel SISO channels satisfying $\widetilde{\mathrm{y}}_i = \sqrt{\frac{E_s}{N_T}}\sqrt{\lambda_i}\widetilde{\mathrm{s}}_i + \widetilde{\mathrm{n}}_i,\ i = 1, 2, ..., r$, where λ_i $(i = 1, 2, ..., r)$ are the positive eigenvalues of $\mathbf{HH}^H$.

The capacity of the MIMO channel is the sum of the individual parallel SISO channel capacities and is given by $\mathbf{C} = \sum_{i=1}^{r} \log_2(1+\frac{E_s\gamma_i}{N_T n_0}\lambda_i)$, where $\gamma_i = \mathbf{E}\{|\mathrm{s}_i|^2\}$ $(i = 1, 2, ..., r)$ reflects the transmit energy in the ith subchannel and satisfies $\sum_{i=1}^{r}\gamma_i =$

N_T.

In an optimal situation, we use $\mathbf{U}$ and $\mathbf{V}$ as our receiver and transmitter beamformers for each deterministic channel matrix $\mathbf{H}$. With $\widetilde{\mathbf{y}} = \mathbf{U}^H\mathbf{y}$, $\widetilde{\mathbf{s}} = \mathbf{V}^H\mathbf{s}$, and $\widetilde{\mathbf{n}} = \mathbf{U}^H\mathbf{n}$, the effective input-output relation for this system is given by $\widetilde{\mathbf{y}} = \sqrt{\frac{E_s}{N_T}}\mathbf{\Sigma}\widetilde{\mathbf{s}} + \widetilde{\mathbf{n}}$.

The MIMO selection process is just choosing two subchannels with the highest λ_i. Normally, the beam vectors are the first two columns of $\mathbf{U}$ and $\mathbf{V}$ at the receiver and transmitter.

This selection needs to calculate the receiver beamformer $\mathbf{U}$ and the transmitter beamformer $\mathbf{V}$ for every deterministic channel matrix. Therefore, it is not practical. But the performance of MIMO selection with such a beamformer is still interesting. We can know how much the MIMO selection performance can be increased theoretically. In this thesis, we call such optimal MIMO selection the "mode selection."

From the previous section, we know that the Weichselberger model gives the best channel capacity estimation with measured channel data. So, if we utilize such a model's idea to create a novel beamformer, which describes the joint spatial structure and adopts the spatial eigenbases to the channel, we should have a higher possibility of choosing the right beam.

The spatial correlation on one link end is denoted by a one-side correlation matrix. Because the two link ends cannot be considered independent, the one-side correlation matrices have to be parameterized by the statistical signal properties of the other link ends:

$$\mathbf{R}_{\mathbf{RX},\mathbf{Q_{TX}}} = \mathbf{E}_{\mathbf{H}}\{\mathbf{H}\mathbf{Q_{TX}}\mathbf{H}^{\mathbf{H}}\},\ \mathbf{R}_{\mathbf{TX},\mathbf{Q_{RX}}} = \mathbf{E}_{\mathbf{H}}\{\mathbf{H}^{\mathbf{T}}\mathbf{Q_{RX}}\mathbf{H}^{*}\}, \tag{45}$$

where $\mathbf{Q_{RX}}$ and $\mathbf{Q_{TX}}$ are the spatial signal covariance matrices of the receiver and transmitter, respectively. Their eigenbases are denoted by $\mathbf{U_{RX}}$ and $\mathbf{U_{TX}}$. The vectors $\overrightarrow{\lambda}_{\mathbf{RX}}$ and $\overrightarrow{\lambda}_{\mathbf{TX}}$ consist of the square roots of the eigenvalues of $\mathbf{R_{RX}}$ and $\mathbf{R_{TX}}$, respectively. Now we use $\mathbf{U_{RX}}$ and $\mathbf{U_{TX}}$ as our fixed receiver and transmitter beamformers. We call the MIMO beam selection with such beamformers the "eigen

selection." Of course, we call the beam selection with the Butler matrix the "Butler selection."

Figure 27 shows the average channel capacity for 8-2 selection at the transmitter only. In Figure 27 (a), the selection is conducted for high-correlated channel T2-R3, while in Figure 27 (b), the selection is conducted for low-correlated channel T2-R2.

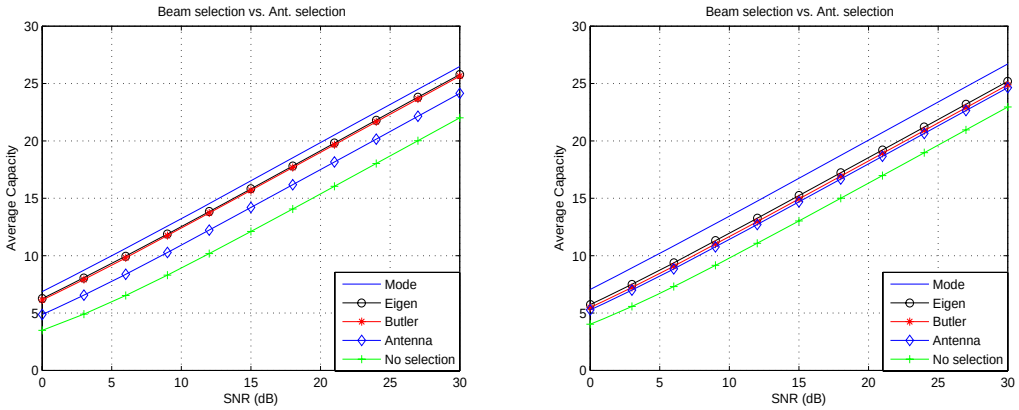

(a) High-correlated MIMO link T2-R3 (b) Low-correlated MIMO link T2-R2

Figure 27: 8-2 selection at the transmitter only for high- and low-correlated MIMO links.

We can see in both figures that the mode selection always has the highest average capacity. The eigen selection is a little better than the Butler selection. All the beam selection methods are better than the antenna selection, and MIMO channel has the lowest average capacity without selection. In a high-correlated MIMO channel, the two practical beam selection methods (eigen selection and Butler selection) are much better than antenna selection, while in low-correlated MIMO channel, the performance of the practical beam selection methods is close to the antenna selection. Such observation again proves the results in Chapter IV.

Figure 28 shows the same results of Figure 27 except that the selection is conducted at both the transmitter and receiver. We can see that the gaps between every curve are increased, which makes it easier to observe the results.

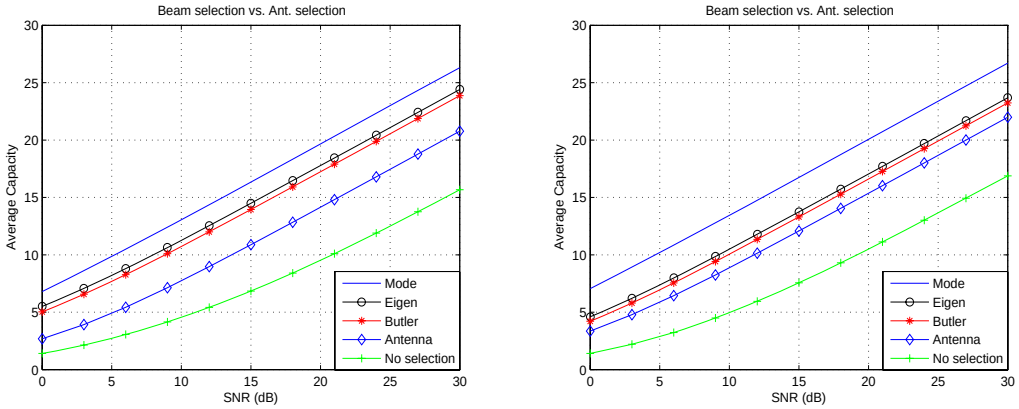

(a) High-correlated MIMO link T2-R3 (b) Low-correlated MIMO link T2-R2

Figure 28: 8-2 selection at both the transmitter and receiver for high- and low-correlated MIMO links.

Through the above analysis, we can conclude that the eigen selection is a little better than the Butler selection. But the improvement is very limited. Compared with the optimal case——the mode selection,——there is still some room for future practical beamformer design.

CHAPTER VI

RESEARCH CONCLUSION

This thesis evaluates the performance of low-complexity antenna or beam subset selection methods for small MIMO networks. The types of networks include (1) point-to-point MIMO links with out-of-system interference and (2) multi-user networks with a single, but possibly spatially distributed access point.

For the first type of network, we propose a new practical selection metric, the peak-to-trough ratio of orthogonal frequency division multiplexing (OFDM) training symbols. We describe our mutibeam receive system and the principle of the PTR metric beam selection algorithm. Combined with RSSI selection, the PTR metric will select beams that have both good desired signal gain and little probability of including large noise and interference. Through analysis and simulation, we found that the PTR metric is robust to synchronization offsets for 802.11a and 802.16a waveforms. The dual-metric (RSSI and PTR) selection method is a good choice for systems with high SNR or low SIR.

We also evaluate various selection techniques on measured indoor channels, which has not been done before. We compare multi-user MIMO systems with selection over a set of measured indoor wireless channels. We analyze the SER performance improvement caused by the joint selection with some popular selection criteria. There is a significant SER gap between the optimal selection criterion (MSER) and both the MCC and the MMSV selection criteria for the high-correlated measured indoor channels, suggesting that improved sub-optimal selection criteria might be possible for this type of channel. Beam selection gives different gains over antenna selection in

different indoor environments. The correlation level is the main reason for this difference. We also compare the non-distributed and distributed receivers. We observe that distributed receivers give an extra macroscopic diversity gain over a non-distributed receiver in the high-correlated channels. In the low-correlated channels with a few strong clusters, we can improve SER performance by either using distributed receivers with antenna selection or adding a beamformer at a non-distributed receiver to conduct beam selection. With these observations, a new MIMO selection architecture guide, considering both the system complexity and the SER performance, is proposed.

Finally, we consider some channel modeling issues associated with beamformers. We investigate the validity of three types of statistical MIMO channel models. In line-of-sight MIMO scenarios, the Weichselberger model is much better than the Kronecker model and the virtual channel representation. In other cases, the Weichselberger model is slightly better than Kronecker model and the virtual channel representation. A new beamformer is designed based on the ideal of the Weichselberger model. The eigen selection is a little better than the Butler selection. But the improvement is very limited. Compared with the optimal case——the mode selection,——there is still some room for future practical beamformer design.

REFERENCES

[1] 802.11a, *Part 11: Wireless LAN Medium Access Contol (MAC) and Physical Layer PHY Specifications*. LAN/MAN Standards Committee, 1999.

[2] 802.16a/D4 2002, *Part 8: Physical Layer*. LAN/MAN Standards Committee, 2002.

[3] Alamouti, S. M., "A Simple Transmit Diversity Technique for Wireless Communications," *IEEE Journal on Selected Areas in Communications*, vol. 16, pp. 1451–1458, Oct. 1998.

[4] Anreddy, V. and Ingram, M., "Capacity of Measured Rician and Rayleigh Indoor MIMO Channels at 2.4 GHz with Polarization and Spatial Diversity," *IEEE Wireless Communications and Networking Conference*, vol. 2, pp. 946–951, April. 2006.

[5] Berenguer, I. and Wang, X., "MIMO Antenna Selection with Lattice-reduction-aided Linear Receivers," *IEEE Transactions on Vehicular Technology*, vol. 53, pp. 1289–1302, Sept. 2004.

[6] Bliss, D. W., Forsythe, K. W., Hero, A. O., and Yegulalp, A. F., "Environmental Issues for MIMO Capacity," *IEEE Transactions on Signal Processing*, pp. 2128–2142, Sept. 1998.

[7] Caldwell, F., Kenney, J. S., and Ingram, M. A., "Design and Implementation of a Switched-beam Smart Antenna for an 802.11b Wireless Access Point," *IEEE Radio and Wireless Conference*, pp. 55–58, Aug. 2002.

[8] Catreux, S., Driessen, P. F., and Sollenberger, N. R., "Simulation Results for an Interference Limited Multiple-input Multiple-output Cellular System," *IEEE Communications Letters*, vol. 4, Nov. 2000.

[9] Chizhik, D., Foschini, G. J., Gans, M. J., and Valemela, R. A., "Capacities of Multi-element Transmit and Receive Antennas: Correlations and Keyholes," *IEEE Electronic Letters*, vol. 36, pp. 1099–1100, June 2000.

[10] Chung, S. T., Lozano, A., and Huang, H. C., "Approaching Eigenmode BLAST Channel Capacity Using V-BLAST with Rate and Power Feedback," *Vehicular Technology Conference*, vol. 2, 2001.

[11] Cimini, L. J., "Analysis and Simulation of a Digital Mobile Channel Using Orthogonal Frequency Division Multiplexing," *IEEE Transactions on Communications*, vol. 33, pp. 665–765, July 1985.

[12] Dong, L. and Ingram, M. A., "Beam Selection Algorithm Based on PTR Metric and Its Synchronization Performance," *IEEE Radio and Wireless Conference*, vol. 1, pp. 115–118, Aug. 2003.

[13] Dong, L. and Ingram, M. A., "Comparing Antenna and Beam Selection for Different Selection Strategies over Measured Indoor MIMO-OFDM Channels at 6 GHz," *12th International Symposium on Antenna Technology and Applied Electromagnetics and Canadan Radio Sciences*, pp. 281–284, July 2006.

[14] Dong, L. and Ingram, M. A., "MIMO Receiver Selection Architectures for Measured Indoor MIMO-OFDM Channels," *Submitted to IEEE Transactions on Wireless Communications*, 2007.

[15] Foschini, G. J., "Layered Space-time Architecture for Wireless Communication in a Fading Environment when Using Multiple Antennas," *Bell Labs Technical Journal*, vol. 1, pp. 41–59, May 1996.

[16] Foschini, G. J. and Gans, M. J., "On Limits of Wireless Communications in a Fading Environment when using Multiple Antennas," *Wireless Personal Communications*, pp. 311–335, 1998.

[17] Gesbert, D., Boleskei, H., Gore, D., and Paulraj, A., "Outdoor MIMO Wireless Channels: Models and Performance Prediction," *IEEE Transactions on Communications*, vol. 50, pp. 1926–1934, Dec. 2002.

[18] Godavarti, M., Hero, A. O., and Marzetta, T. L., "Min-Capacity of a Multiple-Antenna Wireless Channel in a Static Rician Fading Environment," *IEEE Transactions on Wireless Communications*, vol. 4, pp. 1715–1723, July 2005.

[19] Godavarti, M., Marzetta, T. L., and Shamai, S., "Capacity of a Mobile Multiple-Antenna Wireless Link with Isotropically Random Rician Fading," *IEEE Transactions on Information Theory*, vol. 49, pp. 3330–3334, Dec. 2003.

[20] Golden, G. D., Foschini, G. J., Valenzuela, R. A., and Wolniansky, P. W., "Detection Algorithm and Initial Laboratory Results Using the V-BLAST Space-time Communication Architecture," *IEEE Electronic Letters*, vol. 35, pp. 14–16, Jan. 1999.

[21] Gore, D. A., Heath, R. W., and Paulraj, A. J., "Transmit Selection in Spatial Multiplexing Systems," *IEEE Communications Letters*, vol. 6, pp. 491–493, Nov. 2002.

[22] Gore, D. A. and Paulraj, A. J., "MIMO Antenna Subset Selection with Space-time Coding," *IEEE Transactions on Signal Processing*, vol. 50, pp. 2580–2588, Oct. 2002.

[23] Gorokhov, A., Gore, D. A., and Paulraj, A. J., "Receive Antenna Selection for MIMO Spatial Multiplexing: Theory and Algorithms," *IEEE Transactions on Signal Processing,*, vol. 51, pp. 2796–2807, Nov. 2003.

[24] Heath, R. W. and Paulraj, A. J., "Switching between Spatial Multiplexing and Transmit Diversity Based on Constellation Distance," *In proc. of Allerton Conference on Communication*, Oct. 2000.

[25] Heath, R. W. and Paulraj, A. J., "Antenna Selection for Spatial Multiplexing Systems Based on Minimum Error Rate," *IEEE International Conference on Communications*, vol. 7, pp. 2276–2280, June 2001.

[26] Heddergott, R. and Leuthold, P., "An Extension of Stochastic Radio Channel Modeling Considering Propagation Environments with Clustered Multipath Components," *IEEE Transactions on Antennas and Propagation*, vol. 51, pp. 1729–1739, Aug. 2003.

[27] Jeong, W.-C. and Chung, J.-M., "Enhanced Broadband Wireless Networking through Macroscopic Diversity Combining Applications of MIMO Technology," *Conference Record of the Thirty-Eighth Asilomar Conference on Signals, Systems and Computers*, vol. 2, pp. 1458–1462, Nov. 2004.

[28] Jiang, J.-S. and Ingram, M. A., "Enhancing Measured MIMO Capacity by Adapting the Locations of the Antenna Elements," *IEEE International Symposium on Personal, Indoor and Mobile Radio Communications*, vol. 3, pp. 1027–1031, Sept. 2002.

[29] Jiang, J.-S. and Ingram, M. A., "Comparison of Beam Selection and Antenna Selection Techniques in Indoor MIMO Systems at 5.8 GHz," *IEEE Radio and Wireless Conference*, vol. 1, pp. 179–182, Aug. 2003.

[30] Kermoal, J. P., Schumacher, L., Pedersen, K. I., Mogensen, P. E., and Frederiksen, F., "A Stochastic MIMO Radio Channel Model With Experimental Validation," *IEEE Journal on Selected Areas in Communications*, vol. 20, pp. 1211–1226, Aug. 2002.

[31] Lee, W. C. Y., "An Optimum Solution of the Switching Beam Antenna System," *IEEE Vehicular Technology Conference*, vol. 1, pp. 170–172, May 1997.

[32] Li, K.-H. and Ingram, M. A., "Space-time Block-coded OFDM Systems with RF Beamformers for High-speed Indoor Wireless Communications," *IEEE Transactions on Communications*, vol. 50, pp. 1899–1901, Dec. 2002.

[33] Li, K., *RF Beamformers for High-speed Wireless Communication*. Ph.D Thesis, Georgia Institute of Technology, 2000.

[34] Matsumoto, T., Nishioka, S., and Hodder, D. J., "Beam-selection Performance Analysis of a Switched Multibeam Antenna System in Mobile Communications Environments," *IEEE Transactions on Vehicular Technology*, vol. 46, pp. 10–20, Feb. 1997.

[35] Molisch, A. F., Win, M. Z., and Winters, J. H., "Capacity of MIMO Systems with Antenna Selection," *IEEE Transactions on Wireless Communications*, vol. 4, pp. 1759–1772, July 2005.

[36] Molisch, A. F. and Zhang, X., "FFT-Based Hybrid Antenna Selection Schemes for Spatially Correlated MIMO Channels," *IEEE Communications Letters*, vol. 8, pp. 36–38, Jan. 2004.

[37] Moorti, T. and Paulraj, A. J., "Performance of Switched Beam Systems in Battlefield TDMA Networks," *Military Communications Conference, Conference Proceedings, IEEE*, vol. 1, pp. 215–219, Oct. 1996.

[38] Öcelik, H., Herdin, M., Weichselberger, W., Wallace, J., and Bonek, E., "Deficiencies of the "Kronecker" MIMO Radio Channel Model," *IEEE Electronic Letters*, vol. 39, pp. 1209–1210, Aug. 2003.

[39] Pattan, B., *Robust Modulation Methods and Smart Antennas in Wireless Communication*. Prentice Hall PTR, 2000.

[40] Pedersen, K. I., Andersen, J. B., Kennoal, J. P., and Mogensen, P., "A Stochastic Multiple-Input-Multiple-Output Radio Channel Model for Evaluation of Space-Time Coding Algorithms," *IEEE Vehicular Technology Conference*, vol. 2, pp. 893–897, Sept. 2000.

[41] Perini, P. L. and Holloway, C. L., "Angle and Space Diversity Comparisons in Different Mobile Radio Environments," *IEEE Transactions on Antennas and Propagation*, vol. 46, pp. 764–775, June 1998.

[42] Salzand, J. and Winters, J. H., "Effect of Fading Correlation on Adaptive Arrays in Digital Mobile Radio," *IEEE Transactions on Vehicular Technology*, vol. 43, pp. 1049–1057, Nov. 1994.

[43] Sayeed, A. M., "Deconstructing Multiantenna Fading Channels," *IEEE Transactions on Signal Processing*, vol. 50, pp. 2563–2579, Oct. 2002.

[44] Shi, H., Katayama, M., Yamazato, T., Okada, H., and Ogawa, A., "An Adaptive Antenna Selection Scheme for Transmit Diversity in OFDM Systems," *IEEE Vehicular Technology Conference*, vol. 4, pp. 2168–2172, Oct. 2001.

[45] Shiu, D.-S., Foschini, G. J., Gans, M. J., and Kahn, J. M., "Fading Correlation and Its Effect on the Capacity of Multielement Antenna Systems," *IEEE Transactions on Communications*, vol. 48, pp. 502–513, March 2000.

[46] Shiu, D.-S., Foschini, G. J., Gans, M. J., and Kahn, J. M., "Fading Correlation and Its Effect on the Capacity of Multielement Antenna Systems," *IEEE Transactions on Communications*, vol. 48, pp. 502–513, March 2000.

[47] Weichselberger, W., Herdin, M., Öcelik, H., and Bonek, E., "A Stochastic MIMO Channel Model With Joint Correlation of Both Link Ends," *IEEE Transactions on Wireless Communications*, vol. 5, pp. 90–100, Jan. 2006.

[48] Weinstein, S. B. and Ebert, P. M., "Data Tansmission by Frequency Division Multiplexing Using the Discrete Fourier Transform," *IEEE Transactions on Communications*, vol. 19, pp. 628–634, Oct. 1971.

[49] Winters, J. H., "Smart Antennas for Wireless Systems," *IEEE Personal Communications*, vol. 5, pp. 477–482, Feb. 1998.

VITA

Lu Dong was born in 1976 in Nanjing, China. He received his B.S. and M.S. degrees in Southeast University, Jiangsu, China, in June 1998 and March 2001, respectively. In April 2003, he received his second M.S. degree from Georgia Institute of Technology, GA, USA. All the degrees are in Electrical and Computer Engineering. Since the summer of 2003, he has been pursuing the Ph.D. degree in the School of Electrical and Computer Engineering, Georgia Institute of Technology. His research interests include array signal processing, communication systems, information theory, random processes, and RF systems.